공학박사 학위논문

Preparation of patterned membrane and its application to membrane process for Water and Wastewater Treatment

수 처리용 패턴형 분리막의 제조 및 분리막 공정에의 응용

2014년 2월

서울대학교 대학원

화학생물공학부

원 영 준

Abstract

Preparation of patterned membrane and its application to membrane process for Water and Wastewater Treatment

Young-June Won

School of Chemical and Biological Engineering

The Graduate School

Seoul National University

Recently, patterned membrane has proven its potential as an innovative approach to control membrane fouling in the diverse membrane process for production of high quality water. However, preparation steps for diverse patterned membranes are not yet to be established and antifouling mechanism of patterned membrane still remained a black box. In this study, with an aid of soft-lithographic method, a modified preparation step for diverse patterns was developed and antifouling mechanism of patterned membrane in membrane process was discussed.

Firstly, we designed a new preparation step for the patterned membrane.

During the preparation steps, a conventional phase inversion method was converged with a soft-lithographic method, which was applicable to diverse types of pattern. The modified phase inversion method for the patterned membrane could relieve successfully the problem of the reversed pore structures of a conventional method. The relations between preparation parameters and pattern fidelity were estimated.

Secondly, characterization of the patterned membrane was carried out. The pore size distribution and membrane structures of patterned membrane prepared by modified phase inversion method were investigated. After that, the patterned membranes were applied to lab-scale MBR system and the anti-fouling ability of patterned membrane was evaluated.

Lastly, the diverse shape and size of prism-pattern were tested to indentify the antifouling mechanism of the patterned membrane. We developed diverse patterns such as interval prism pattern and have investigated deposition of latex particle in response to change of Reynolds number or particle diameter. Comparing the mass of attached particle on diverse prism pattern with non-patterned case, the parameters affecting antifouling ability of patterned membrane were investigated.

Keywords

Water treatment, wastewater treatment, patterned membrane, membrane fouling, Soft-lithography, Phase inversion

Student Number: 2007-30850

Table of Contents

List of Figures

List of Tables

Chapter I

Introduction

I.1. Backgrounds

Over the past two decades, a membrane bioreactor (MBR) where a biological activated sludge process is combined with membrane filtration has emerged as an innovative technology for the effective wastewater treatment and reuse. The membrane application in bioreactors can overcome the disadvantages of the sedimentation tanks that are used in most biological treatment systems. In addition, MBRs offer a number of advantages over the conventional activated sludge process, such as excellent quality effluent, a more compact treatment facility, a more concentrated biomass, and a reduced sludge yield. With its increasing application, the MBR process has demonstrated its potential to fundamentally advance the technology and practice of wastewater treatment and water reclamation. For example, more than 4,400 MBR plants have been installed worldwide by the end of 2009 (Judd and Judd 2011). However, the application of MBR has been hampered, particularly by membrane fouling, which is closely associated with the naturally attached microbial growth on the membrane surface (Hwang et al. 2008, Drews 2010). Especially, biofouling control has been a critical research issue as around 60 % of MBR operating cost is directly related to biofouling (Judd and Judd 2011). Therefore, tremendous efforts to inhibit biofouling in membrane processes for water treatment have been made through engineering, material, and chemistry platforms (Drews 2010, Xiong and Liu 2010).

Recently, novel approaches have been attempted to mitigate membrane

fouling from the view point of converging science. Among them, the study of membrane topography was shed new light on the control of membrane fouling. Usually, the membrane topography simply indicated the roughness of membrane surface and moreover the higher roughness was deemed to aggravate the membrane fouling. However, with the development of patterning technique, diverse patterned surfaces were tested for their potential mitigating the deposition of foulants. As a result, some effects of patterned surface on the control of membrane fouling have been suggested: i) the patterned surface can promote the turbulence and thus reduce the membrane fouling ii) the flux of membrane was significantly augmented because the effective membrane area increased by patterning. Culfaz et al. prepared a patterned hollow fiber membrane by a patterned spinnerette and observed that the patterned membrane exhibited higher water flux than that of the conventional hollow fiber membrane.(Culfaz et al. 2011a, Culfaz et al. 2011b, Culfaz et al. 2010, Culfaz et al. 2011c, d) They also found that the fouling resistances of structured fibers were better than those of normal hollow fibers under specific conditions. Although their work demonstrated that remarkable improvement in the membrane fouling could be possible with a patterned surface, it is difficult to fabricate smaller and diverse patterns by spinning hollow fiber membrane through a spinnerette. Efimenko et al. also prepared marine coatings comprising hierarchically wrinkled surface topographies with wrinkles of different length scales ranging from tens of micrometer to a fraction of a millimeter and investigated the behavior of foulants at such small size (1 – 100 μm) patterned

surface.(Efimenko et al. 2009) They demonstrated that the wrinkled surface remained relatively free of biofouling even after prolonged exposure to seawater whereas a flat surface did not. The wrinkled surface, however, was not a porous membrane but PDMS surface. Therefore more effective preparation method for patterned membrane and analysis of antifouling mechanism of patterned membrane are required for the successful biofouling control in real MBR.

I.2. Objectives

The objective of this study was to devise the new preparation steps for patterned membrane and investigate the inhibition of membrane fouling in MBR by the pattern formed on membrane surface. The specific objectives of this study are as follows:

(1) Designing a new preparation steps for patterned membrane

In order to prepare the diverse patterned membranes, a new modified phase inversion process was developed. Also the parameters affecting pattern fidelity was indentified.

(2) Characterization and application of patterned membrane to membrane process

The pore size distribution and membrane structures of patterned membrane prepared by modified phase inversion method were investigated. After that, the patterned membranes were applied to lab-scale MBR system and the antifouling ability of patterned membrane was evaluated.

(3) Comparing diverse prism pattern to elucidate the antifouling mechanism of patterned membrane

With aid of soft-lithographic methods, the diverse shape and size of pattern

were tested. These diverse patterned membranes were applied to lab-scale membrane process and the membrane fouling of each patterned membrane was investigated.

Chapter II

Literature Review

II.1. Phase inversion methods

II.1.1.Introduction

Polymeric membranes have been developed for a variety of industrial applications. Examples of industrial applications are micro-filtration, ultra-filtration, reverse osmosis and gas separation. Each application imposes specific requirements on the membrane material and membrane structure.

There are several ways to prepare porous polymeric films, such as sintering, stretching, track etching and phase separation process. Among them, the phase inversion (PI) methods are the leading method for the preparation of polymeric membranes with a porous bulk part because the membrane is prepared very quickly and easily by PI method.(vandeWitte et al. 1996a) The changes in composition can be achieved either by the introduction of new species or through the selective removal of species. The introduction of new species is usually accomplished by immersion of the dope in a bath that is solvent-miscible but a non-solvent of the polymer. PI through the removal of dope species involves dopes containing a volatile solvent and a non-volatile non-solvent. In both cases the change in composition brings the solution within a multiphase region of the phase diagram. PI membrane can be categorized into two groups. I) symmetric (morphology is fixed along the thickness) or ii) asymmetric (morphology varies substantially along the thickness). While early PI research focused almost exclusively on polymers with limits or no capacity for crystallization, in 1987 the

additional structural options offered by the processing of dopes of crystallizable polymers have led to the establishment of widely pursued new directions in PI research.(Reuvers and Smolders 1987, Reuvers et al. 1987)

II.1.2.Non-solvent induced phase inversion (NIPs) method

II.1.2.1. Introduction

Membrane formation by immersion precipitation has been studied much less intensively than thermally induced phase separation. Nevertheless, a good picture of the process is now available. A schematic representation of membrane formation by immersion precipitation is presented in Figure II-1. Immersion precipitation is more complicated than thermally induced phase separation, because at least three components are involved, and because complex diffusion and convection processes play an important role. Only ternary combinations of polymers, solvents and non-solvents will be discussed. From the earlier discussion on binary systems, it is clear that a large number of phase transitions and combinations of phase transitions can play a role. Introducing a third component will make the phase diagrams even more complex. Fortunately, the complexity is reduced by the fact that the immersion precipitation process can be regarded as an isothermal process. As opposed to binary systems, ternary systems are discussed in the literature almost exclusively in relation to generating porous morphologies. Liquid-liquid demixing plays a central role in this process. Therefore other phase transitions (vitrification) and solid-liquid demixing and gelation (crystallization of the polymer) will not be treated separately but in their relation with liquid-liquid demixing.(Frank and Keller 1988)

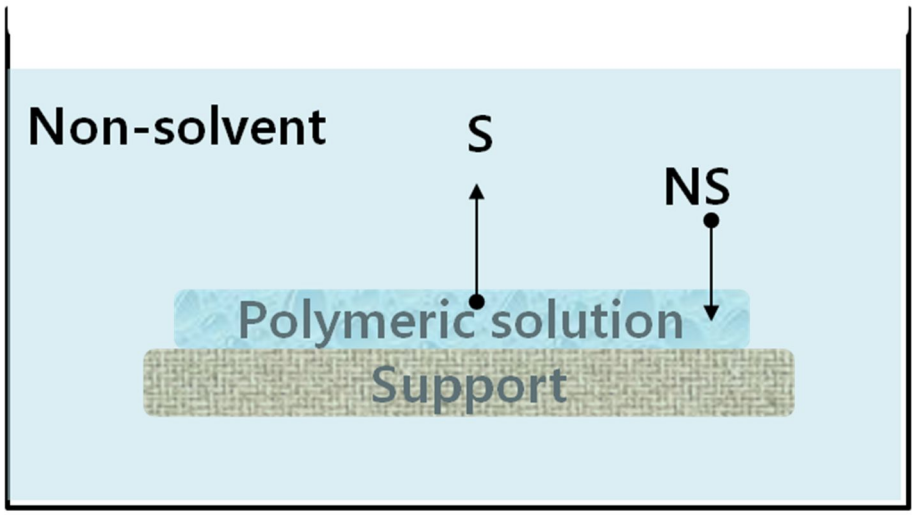

NS : non-solvent
S : solvent

Figure II-1. Schematic diagrams of the immersion precipitation process (vandeWitte et al. 1996a)

II.2.2.2. Preparation steps of NIPs

Immersion precipitation membranes in their most simple form are prepared in the following way. A polymer solution consisting of a polymer and a solvent is cast as a thin film upon a support (e.g. fabric or glass plate) and then immersed in a nonsolvent bath. The solvent diffuses into the coagulation bath whereas the nonsolvent will diffuse into the cast film. After a given period of time the exchange of solvent and nonsolvent has proceeded so far that the solution becomes thermodynamically unstable and demixing takes place. Finally a solid polymeric film is obtained with an asymmetric structure. The local composition at any point in the cast film depends on the time. However, it is not possible to measure composition changes very accurately with time because the thickness of the film is only of the order of a few micrometers. Furthermore, sometimes membrane formation can occur instantaneously, i.e. all the compositional changes must be measured as a function of place and time within a very small time interval. Nevertheless, these composition changes can be calculated. Such calculations provide a good insight into the influence of various parameters upon membrane structure and performance. Different factors have a major effect upon membrane structure. These are:

- Choice of polymer
- Composition of casting solution
- Composition of coagulation bath
- Location of the liquid-liquid demixing gap

- Temperature of the casting solution and the coagulation bath
- Evaporation time
- Choice of solvent and nonsolvent

By varying on or more of these parameters, which are not independent of each other, the membrane structure can be changed form a very open porous form to a very dense nonporous variety. (Reuvers and Smolders 1987, Reuvers et al. 1987, Termonia 1995)

II.2.2.2. Mechanisms of NIPs

An interesting question remains after the membrane preparations. How is it possible to obtain different structure with alone and the same system? In order to understand this, it is necessary to consider how each of the variables affects the phase inversion process. The ultimate structure arises through two mechanisms: 1) demixing processes; and 2) diffusion processes involving solvent and nonsolvent occurring during membrane formation. Thus, demixing processes will first be considered.

All of the possible combinations of three components concerned with NIPs can be plotted in a triangle. The corners represent the pure components, the axes the three binary combinations and a point in the triangle a ternary composition (Figure II-2). The phase diagram is divided into a homogeneous region, and an area representing a liquid-liquid demixing gap. The liquid-liquid demixing gap is entered when a sufficient amount of nonsolvent is present in the solution. In principle, the same three parts of the demixing gap are present as in the binary diagram. A metastable area exists between the spinodal and the binodal at low polymer concentrations, an unstable area is enclosed by the spinodal, and a second metastable area at higher polymer concentrations. The phase separation proceeds analogously with binary solutions.

A line is plotted in the phase diagram which connects the initial composition of the film to the final averaged composition of the film and the coagulation bath. The arrow does not represent the compositional change in the

solution as a function of time. The components in the polymer solution will take a different composition path to the end condition.

In the framework of the Flory-Huggins description of polymer solutions, the size and location of the demixing gap depends on the molar volumes of the components, the polymer-solvent interaction parameter, the polymer-nonsolvent interaction parameter, and the solvent-nonsolvent interaction parameter The influence of these variables on the resulting phase diagrams has been discussed in detail by Altena and Tsay(Altena and Smolders 1982, Yilmaz and Mchugh 1986). The effect of polydispersity of the polymer on these phase diagrams has been discussed by Koningsveld and Kamide (Kamide and Matsuda 1984, Koningsv.R 1972). The influence of the parameters can be summarized as follows.

- A polymer-nonsolvent interaction parameter determines, to a great extent, the surface area of the liquid-liquid demixing gap. High polymer nonsolvent interaction parameters imply that the point of intersection of the demixing gap with the polymer-nonsolvent axis is located at very high polymer concentrations.
- Polymers and solvents with low mutual affinity increase the magnitude of the demixing gap, especially at low values of .
- Low compatibility of solvent-nonsolvent mixtures results in large differences in solvent/nonsolvent ratio in the equilibrium phases. Solvents and nonsolvents with high mutual affinity strongly increase the magnitude of demixing gaps.

In first approximation (minor) changes in molecular weights, molecular weight distributions and molar volumes are negligible compared to the influence of interaction parameters. The number of experimental ternary phase diagrams reported in the literature is limited. Some phase diagrams were determined by Strathmann for polyamides in a number of solvent/nonsolvent mixtures (Strathmann 1985, Strathmann and Kock 1977). For polyurethane in DMF/water mixtures, the liquid-liquid demixing gap was determined by Koenhen et al., the phase behaviour of polysulfones and polyethersulfones in solvent/nonsolvent mixtures was studied by many groups(Koenhen et al. 1977). Ternary phase diagrams for cellulose acetate have also been frequently published (Mulder et al. 1985, Altena et al. 1986, Reuvers et al. 1986). The demixing gap for polyvinylidenedifluoride in some solvent/nonsolvent mixtures was reported by Bottino et al(Bottino et al. 1991). In general, the theoretical predictions for the influence of the parameters on the size and location of the liquid-liquid demixing gap are also found experimentally(VandeWitte et al. 1996b). However, the quantitative correspondence between theoretical phase diagrams and experimental phase diagrams is rarely studied. The determination of interaction parameters is usually rather time consuming. A polymer-nonsolvent interaction parameter is difficult to determine, but can be calculated via swelling measurements(Mulder et al. 1985). Low compatibility of solvent and nonsolvent mixtures can be calculated from activity data in the literature on solvent-nonsolvent mixtures (Altena and Smolders 1982) and polymer and solvents with low mutual affinity can be obtained

from light scattering or osmometry measurements. In addition, vapor sorption can be used for the determination of polymer- solvent and polymer-nonsolvent interaction parameters. A more rapid indication for the (relative) values of some of these parameters can be obtained from intrinsic viscosity measurements, and heats of mixing (usually available in literature). Even more rapid (although only qualitative) is the solubility parameter approach (So et al. 1973).

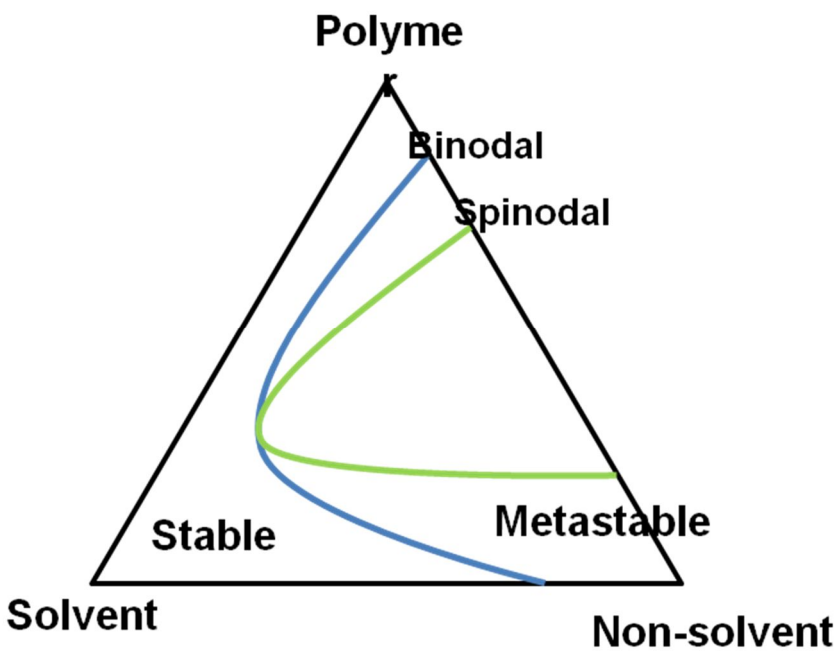

Figure II-2. Example of an isothermal phase diagram for mixtures of a polymer, a solvent and a nonsolvent.

II.2.2.3. Structures of membrane prepared by NIPs

A detailed description of membrane applications and the membrane morphology that is desired for each application is presented in many books. There is a general consensus among researchers that, in the case of immersion precipitation, liquid-liquid demixing processes are largely responsible for the membrane morphology. Nevertheless, the attribution of specific structures in the membrane to phase separation processes is even more complicated for ternary systems than for binary systems. The reason for these difficulties is that the diffusion processes change the initial composition of the film directly after immersion. Also the composition is not the same throughout the solution. The mechanism of formation of the top layer can differ from the mechanism of formation for the layer close to the support. In addition, the lacks of knowledge on coarsening processes complicate the analysis. Because of the much more complex relation between membrane morphology and system parameters for the immersion precipitation process, these relations will be examined in somewhat more detail. A part of the discussion remains useful for the TIPS process. The first part of the discussion is valid for the phase separation of amorphous polymers stabilized by verification and to some extent also other solidification processes. In addition, some attention will be paid to the morphologies obtained for crystalline polymers. Kimmerle distinguished four structural elements in the morphology of membranes obtained by immersion precipitation (Kimmerle and Strathmann 1990):

1. Cellular structures.

2. Nodules.

3. Bicontinuous structures.

4. unconnected latex (filterdust, blushing).

A fifth membrane structure that is frequently observed is the macrovoid. From their micrographs a transition in structural elements can clearly be observed (Manabe et al. 1987). Similar observations were made by Gittens et al.(Gittens et al. 1970). These structures are the same structural elements that have been observed for liquid-liquid demixing in binary systems. This similarity has been recognized by most investigators in membrane formation mechanisms. Nevertheless, different mechanisms have sometimes been proposed for the formation of these structures. The current theories on the origin of the structures will be reviewed in the following section.

Almost all membranes prepared by delayed precipitation have an open or closed cell structure in the sublayer. Smolders and co-workers demonstrated convincingly that nucleation and growth of a polymer poor phase is responsible for the pore generation (Broens et al. 1977). In combination with the developed transport model and the phase diagrams, they were able to predict trends for the membrane structures as a function of various variables (Reuvers and Smolders 1987, Reuvers et al. 1987). The delay time for demixing is an important parameter in determining the membrane morphologies. Earlier in the paper the division was made between membrane morphologies obtained by rapid demixing and delayed demixing. The delay time is in the order of one second or less for rapid demixing

conditions. For delayed demixing the precipitation time is in the order of seconds to minutes. Under rapid demixing conditions, membranes can be expected with a very thin top layer and a sub-layer with a lot of macrovoids. The top layer of these membranes often consists of nodular structures and possesses some degree of porosity. The membrane will generally possess ultra-filtration or hyper-filtration properties, and is suitable for separation of small particles, high molecular weight components or salts from low molecular weight compounds. For membranes obtained by delayed demixing, the top layer will be very dense and thick. Because of the high concentration of the polymer solution at the onset of demixing, the porosity and the degree of interconnectivity of the pores will be low. The permeability of the membranes is generally low. If the resistance of the sub-layer can be kept low, the membranes are in principle suitable for applications based on hyper-filtration, gas separation, and reverse osmosis. For these applications, membranes with a defect free ultrathin dense top layer and a sub-layer with a high porosity and good interconnectivity of the pores are desired. The trends in membrane morphology can be predicted using this table and the general remarks that were mentioned earlier in this section. The influence of the composition of the casting solution and coagulation bath on the membrane morphology cannot be fully explained in terms of delay time. The delay time will decrease when nonsolvent is added to the polymer solution. In addition, the size of the top layer will decrease. The pore size of the membrane also decreases with increasing polymer concentration. Close to the transition from delayed demixing to rapid demixing,

macrovoids will be obtained. When the nonsolvent concentration is very high, the conditions for macrovoid formation worsen. In the model of Reuvers, the skin thickness of the nascent membrane is insufficient to sufficiently decrease the inflow of nonsolvent. Within a short period of time, demixing occurs throughout the polymer solution (Reuvers and Smolders 1987, Reuvers et al. 1987). The delay time will increase when solvent is added to the coagulation bath. The polymer concentration at the interface will decrease, and facilitate phase separation in the top layer or growth of the polymer poor droplets through the interface. Wijmans demonstrated that membranes with a porous top layer can be obtained when the concentration of solvent in the coagulation bath exceeds a certain minimum value. This minimum concentration is determined by the nonsolvent power. In addition, macrovoids can disappear, and thinner top layers can be obtained. Fibres with porous inner top layers are easily obtained by adding solvent to the bore liquid.

The fixation of the membrane structure will also be delayed, because of the depression of the glass transition of the polymer by the solvent. Coarsening can continue for a longer time period, and the pores will become larger. Increasing polymer concentrations will increase the thickness of the top layer and decrease the porosity of the membrane and the interconnectivity of the pores. The macrovoid formation will be diminished, and the pore size will increase. The polymer concentration of the casting solution also plays a role in determining the importance of other phase transitions

Membranes that consist, as a whole, of a highly interconnected pore

structure, or contain a layer with a highly interconnected pore structure, were prepared. These interconnected pore structures can be due to spinodal decomposition, or can be the result of coalescence of polymer poor droplets generated by binodal decomposition. Kesting and Kamide suggested that these bicontinuous structures can be due to the aggregation of nodules (Kesting 1990, Zhenxin and Matsuura 1991). It has been argued that spinodal demixing during membrane formation is not very likely. Two reasons for this have been given. First of all, according to the mass transport model theories, the driving force for diffusion becomes zero at the spinodal (Vitagliano et al. 1978, Radovanovic et al. 1992a, b). Secondly, Wijmans and Smolders state that binodal demixing is usually sufficiently rapid to prevent the composition of the solution from reaching the spinodal. Binder states that the binodal decomposition process and the spinodal decomposition will resemble each other in the vicinity of the spinodal. It is possible that open structures can also be obtained by deep quenches in the metastable area. Still, if the cellular structures can be attributed to the nucleation and growth of polymer poor phase and the nodules to nucleation and growth of polymer rich phase, it seems reasonable to attrite the intermediate bicontinuous layer to spinodal decomposition. An additional argument for the gradual change in decomposition mechanism is that the bicontinuous structures often contain spheres. Nevertheless, these discussions remain hypothetical and more experiments have to be performed in order to resolve this issue.

II.1.3. Thermally induced phase inversion (TIPs) method

II.2.2.1. Introduction

Membrane fabrication via TIPS offers several advantages relative to conventional casting processes such as greater flexibility, ease of control, a low tendency for defect formation, effective control of the final pore size, and the ability to generate both isotropic and anisotropic structures. In particular, TIPS enables very high porosities to be obtained since the diluent that dissolves the polymer at high temperatures becomes a nonsolvent pore-former when the casting solution is cooled. For this reason the diluents used in TIPS-casting are referred to as latent solvents.

The TIPS process has been used to fabricate membranes from many different sparingly soluble polymers. Although TIPS is conceptually a simpler process than conventional wet-casting, it is a complex process to model since it involves coupled heat and mass transfer leading to very rapid phase separation and solidification. Depending on the polymer solution properties and casting conditions, phase separation can occur via one or more mechanisms including liquid–liquid (L–L), solid–liquid (S–L), liquid–solid (L–S), and solid–solid (S–S) demixing. Because of this complexity, relatively few theoretical models have been advanced to describe the TIPS process. Caneba and Soong advanced the first model for the TIPS process whereby they described L–L phase separation via spinodal composition (Caneba and Soong 1985). A mathematical model for nucleation and growth during S–L TIPS-casting was developed by Li et al. (Li et al. 2006).

Recently Hanks and Lloyd advanced the first model to describe the evolution of the membrane structure that occurs after isothermal droplet coarsening in L–L TIPS (Hanks and Lloyd 2007). Although these modeling studies provide considerable insight into the physicochemical processes that occur during TIPS, advances in the development of the TIPS process have come primarily from extensive experimental studies.

The commercial potential of TIPS-casting of sparingly soluble polymers has been known for quite some time as evidenced by a series of early patents. These patents describe new membranes fabricated via TIPS from different polymer/latent solvent systems but do not discuss any in-depth experimental studies.

Hiatt et al. published one of the first in-depth studies of TIPS-casting (Hiatt et al. 1984, Hiatt et al. 1985). Their studies for the polypropylene/N,N-bis-(2-hydroxyethyl) tallowamine system demonstrated that the membrane structure and properties are controlled by the choice of polymer/diluent system, solution concentration, solution temperature, and cooling rate. Another early experimental study was that of Caneba and Soong who considered L–L TIPS for poly(methyl methacrylate)/sulfolane casting solutions (Caneba and Soong 1985).

II.2.2.2. Preparation steps of membranes using by TIPs

In this section, the preparation steps for hollow fiber membrane were discussed. A polymer solution is pumped through the spinneret, where the non-solvent following along the bore forms the lumen of the capillary (or hollow fiber) membrane as it is formed in the coagulation bath by phase inversion. Asymmetric membranes are used primarily in pressure-driven membrane processes such as reverse osmosis, ultrafiltration, or gas separation, as it is here that the unique properties in terms of high mass transfer rates combined with good mechanical stability can be best utilized. In addition to high filtration rates, asymmetric membranes are very resistant to fouling. Conventional symmetric structures act as depth filters and retain particles within their internal structure. These trapped particles plug the membrane and so the flux declines during use. Asymmetric membranes are surface filters and retain all rejected materials at the surface where they can be removed by shear forces applied by the feed solution moving parallel to the membrane surface.

Two techniques are used to prepare asymmetric membranes. The first technique utilized the phase inversion process and leads to a membrane where the skin and the substructure consist of the same polymer. This membrane is referred to as integral asymmetric. IN the second technique, and extremely thin polymer film is deposited on a preformed porous substructure, leading to the so-called composite membranes.

The development of the first integral asymmetric membranes by phase

inversion was a major breakthrough in the development of ultrafiltration and reverse osmosis. These membranes were made from cellulose acetate and yielded fluxes 10- 100 times higher than symmetric structure with comparable separation characteristics. Today, however, most reverse osmosis membranes are composite structure.

II.2.2.3. Mechanisms of membranes using by TIPs

A quantitative treatment considering all thermodynamic and kinetic parameters involved in the phase inversion process is difficult. However, a phenomenological description of the process with the aid of the phase diagram of a mixture consisting of a polymer, one or more solvents, and nonsolvents at constant or different temperatures is very useful for a better understanding of the relation between membrane structure and the different preparation parameters. However, it must be realized that the phase diagram is the thermodynamic description of an equilibrium state. In the membrane formation process, the phase separation is also determined by kinetic parameters, and thermodynamic equilibrium is generally not obtained on a macroscopic scale. The quantitative description of the kinetics is difficult. However, just a general thermodynamic description of the phase separation based on the phase diagram of the polymer/solvent/nonsolvent system provides valuable information concerning the membrane structures obtained by the phase inversion process

The temperature-induced phase separation of a two-component polymer mixture is illustrated in Figure II-3, which shows a phase diagram of a two-component mixture of a polymer and a solvent as a function of temperature. The diagram indicates a miscibility gap over a wide range of composition at low temperature. Above a certain temperature, the polymer and solvent form a homogenous solution at all compositions. At other temperatures, the system is not stable at certain compositions and will separate into two phases. This region is

referred to as the miscibility gap, which is surrounded by the binodale curve. If a homogeneous polymer-solvent mixture of a certain composition at a temperature T1, as indicated by point A in Figure II-3, is cooled to the temperature T2, as indicated by point B, it will separate into two different phases, the composition of which is indicated by the point B' and B''. The point B'' represents the polymer – rich phase and the point B' the solvent –rich polymer-lean liquid phase. The lines B'-B and B''-B represent the ratio of the amounts of the two phases in the mixture, that is, the overall porosity of the obtained porous system. If the polymer concentration in the polymer-rich phase has reached a certain value, its viscosity is increased to such an extent that it can be considered as solid. The polymer-rich phase forms the solid membrane structure and the polymer-lean phase the liquid-filled pores.

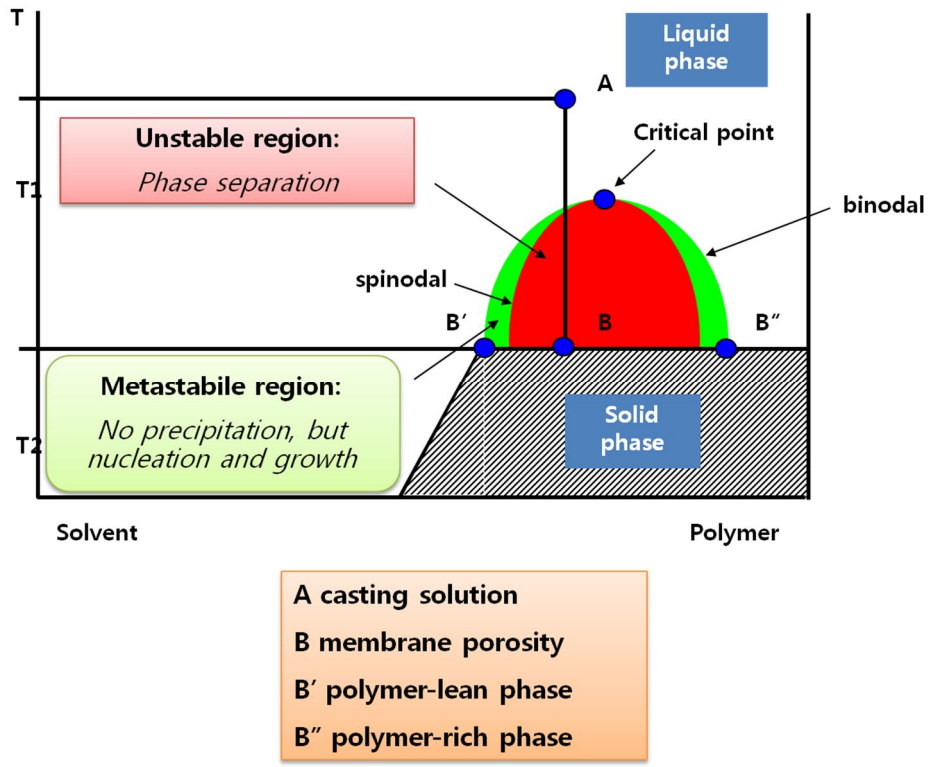

Figure II-3. Schematic diagrams showing the formation of a micro-porous system by a thermal precipitation of a two component mixtrue

II.2. Soft-lithography

II.2.1.Introduction

Soft lithography represents a non-photolithographic strategy based on self-assembly and replica molding for carrying out micro- and nanofabrication. It provides a convenient, effective, and low-cost method for the formation and manufacturing of micro- and nanostructures (Kumar et al. 1994). In soft lithography, an elastomeric stamp with patterned relief structures on its surface is used to generate patterns and structures with feature sizes ranging from 30 nm to 100 μm (Choi et al. 2004). These unconventional nanopatterning techniques are based primarily on the use of molds or stamps. The features of these techniques are largely determined by the properties of the materials used. These properties include surfaces energy, Young`s modulus, transparency to light, and compliance or flexibility. For example, the mold material should have a low surface energy for the mold to be released cleanly and easily form the material being patterned. Similarly, if the material to be patterned is an ultraviolet (UV) curable pre-polymer, the mold should be transparent to the light (Choi et al. 2004).

Thus, the material of stamps is very important for soft lithography, it will be discussed at next section.

II.2.2.Materials for soft -lithography

Nanopatterning can be accomplished with hard, soft or rigiflex molds (Brittain et al. 1998a, Brittain et al. 1998b, Ho et al. 1998, Jeon et al. 1998, Xia and Whitesides 1998). The choice of mold depends on the requirements of the application. A soft mold is typically used for soft lithotraphy, whereas a hard mold is generally used for imprint lithography. A rigiflex mold can be used in place of a hard or soft mold in most cased.

II.3.2.1 Soft molds.

The most representative of soft molds are made from Sylgard 184 (Dow Corining). Molds of this type date back to the first reports of microcontact printing, the first type of soft lithographic technique, in 1993 (Kumar and Whitesides 1993). Such molds are fabricated by casting a mixture of pre-polymer and cross-linker at a recommended ratio of 10:1 against a master with relief structures that correspond to the desired pattern. A curing time of 4-6 h and a curing temperature of 60 C should be used,. A lower ratio fo cross-linker leads to a stickier mold surface.

The Sylgrad PDMS, sometimes referred to as soft PDMS (s-PDMS), has a number of characteristics and physical properties that are well suited for soft lithography. Its surface energy is low at 21 dyn cm-1 and it is transparent in the UV and visible regions. In addition, it has high gas permeability. For example, the permeability is 10 -11 cm2 (s pa)-1. Its flexibility and tackiness allow conformal contact of the mold with the underlying surface. the thermal expansion coefficient

is , however, relatively high at 210 um (m C)-1 such that a linear shrinkage on the order of 1.5% occurs when cooled after curing at 60 C (Schmid and Michel 2000). The mold also has the disadvantage that it swells in many organic solvents as toluene. The modulus of elasticity or Young`s modulus of a PDMS is around 2 MPa, depending on the mixing method, curing time, and temperature. This low modulus limits the fabrication of features with high aspect ratios due to collapse, merging, and buckling of the structure of relief (Hui et al. 2002, Lee et al. 2003, Odom et al. 2002). These deformation modes have been examined both theoretically and experimentally. The theoretical criteria that can be used for dimensional stability and conformity of a mold are summarized in Figure II-4. Conformity here means full contact of the mold feature with the underlying substrate surface. The criteria given in the figure II-4 are such that if they are satisfied then the mold avoids the associated deformation. For instance, if the equation in the first entry of the fig is satisfied, then the mold will not undergo roof collapse. An obvious way to overcome unwanted deformations is to use a mold with a higher Young`s modulus (Sharp et al. 2004). Therefore, there have been attempts to use materials of high Young`s modulus for soft molds. The earliest example use alternative siloxane polymers having a Young`s modulus of around 9 MPa, known as hard PMDS. To overcome the shortcomings of hard PDMS, such as it brittleness, and the need to apply pressure to achieve conformal contact with substrate, a composite mold of PDMS was introduced., in which a thin hard PDMS layer with relief the structure is supported by a thick layer of soft PDMS (Kang et

al. 2006). This composite design combines the advantages of both a more rigid layer (to achieve high resolution patterning) and a more flexible support (to facilitate handling and the establishment of conformal contact)

To further improve the resolution in patterning with a soft mold and to overcome some of the shortcomings of PDMS such as swelling, a commercially available form of perfluoropolyether (PFPE) (CN 400, Sartomer Co,. Mw = 1000 g mol -1) has been explored as a mold material. Unlike certain PFPE formulations described earlier, which have a Young`s modulus of around 3 MPa and have been demonstrated for micro-fluidics device fabrication (Sharp et al. 2004) and imprint lithography (Rolland et al. 2004a, Rolland et al. 2004b), the Young`s modulus of acryloxy PFPE, denoted as a- PFPE, is 10.5 MPa. The low surface energy (-18.5 mNm-1) as well as the chemical inertness of a PFPE eliminates the necessity of treating the surfaces of the masters with fluorinated silanes to avoid sticking during casting and curing of the mold. The resolution capabilities of both a-PFPE and hard PDMS are remarkable (Truong et al. 2007). In recent experiments, they have been used for molecular scale molding where SWNTs with diameters of 1-3 nm act as a templates. Systematic studies show that the resolution for these materials extends nearly to the 1 nm regime, where the ultimate resolution tends to be limited by the surface roughness of the molded patterns. The high resolution capabilities of a-PFPE, together with other properties such as resistance to swelling, chemical inertness, and photo-curability make it a promising alternative to PDMS for certain soft lithographic techniques (Hua et al. 2006, Hua et al. 2004).

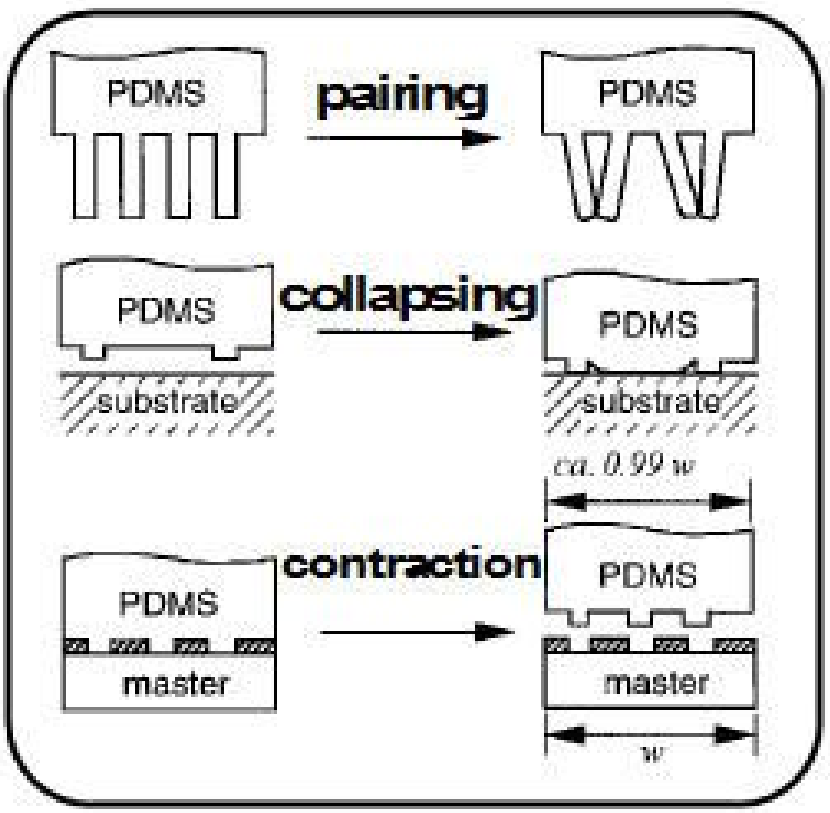

Figure II-4. Schematic diagram of dimensional stability (Rogers and Lee 2009)

II.3.2.2 Hard molds.

Hard molds such as those prepared by photo lithography or electron-beam lithography on silicon wafers are used for nano imprint lithography (NIL) and room temperature imprint lithography (RTIL) (Kumar et al. 1994, Hong and Lee 2003, Khang and Lee 2000, Khang et al. 2001, Ye et al. 2010). The Young`s modulus of these hard molds is high enough to withstand the high applied pressures that are often required for patterning (Ruchhoeft et al. 1999). Patterning by NIL is based on pressure-driven flow of a polymer melt; patterning by RTIL relies on the plastic deformation of polymer. High pressures are required in both cases. By contrast, low pressures are sufficient in step and flash imprinting lithography due the use of low viscosity UV curable liquid pre-polymers in this technique. Quartz molds are typically used for SFIL, due to their high modulus, dimensional stability and transparency in the UV range (Choi et al. 2004).

Unlike soft molds, which can be replicated many times easily and cheaply form a single master, the master template itself is usually used for hard molds. For NIL and RTIL, hard molds in the form of nickel stamps can be replicated from a master. If the master is a silicon mold, a thin metal layer can be coated and nickel electroplating can be carried out to replicate the master. Another method is to deposit a seed layer by electroless deposition, followed by nickel electroplating in a nickel sulfamate solution. For quartz molds used for SFIL, the transparency requirement precludes the method of nickel electroplating for replication (Yoo et al. 2004).

II.3.2.3 Rigiflex molds.

A rigiflex mold is one with a Young`s modulus between several tens of MPa and a few Gpa. This type of mold is rigid enough for high resolution patterning and yet flexible enough in its film form for conformal contact with a surface (Kim et al. 1996). it is noted in this regard that the flexibility is inversely proportional to the product of the Young`s modules and the thickness cubed. Therefore, a 1-um thick sheet with the modulus of 1GPa is as flexible as a 10 um thick sheet with the modulus of 1Mpa. As an example, a 1mm thick Teflon mold, for which the modulus is 1.6 Gpa, is more flexible than a 1 cm thick soft PDMS mold, for which the modulus is around 2.0 MPa. Rigiflex molds based on Teflon and UV curable poly(urethaneacrylate, PUA) have been introduced recently (Khang et al. 2004, Khang and Lee 2004a).

The PUA mold can be prepared by pouring liquid prepolymer (MINs, Minuta Inc.) onto a master template. A flexible and transparent backing layer of PU elastomer or soft epoxy resin is brought into contact with the liquid prepolymer. It is then exposed to UV (250-400 nm) for 2 min at room termperature through the transparent backside. After the curing, it is peeled off from the master. The Young`s modulus of MINS ERM is around 100 MPa and that of MINS 311RM is around 400 MPa. The mold can be self-replicated and its surface energy is around 23 dyn cm-1, which is comparable to that of PDMS (Choi et al. 2004). It is almost impermeable to gases, inert to chemicals and solvents such that there is no swelling problem, and it is transparent to light in the UV and visible regions. Because of the

rigiflex nature of the mold and the tenability of the modulus, it can be used not only for micro-contact printing but also for imprinting.

II.2.3.Diverse patterning techniques of soft-lithography

II.3.3.1 Soft molding

The soft molding process is a soft lithography technique by solvent-induced capillarity using soft elastomeric mold (Choi and Rogers 2003). Soft molding was developed to substantially reduce the high pressure needed for molding by using a soft mold that is capable of absorbing the solvent from sufficiently solvent-contained polymer film by the time the polymer is molded (Kim et al. 2001). However, the PDMS molds typically used in previous work on soft molding has generally difficulty in producing a densely arrayed nanopattern(e.g., alternating 100 nm line and space) because the PDMS mold collapses laterally as pointed out before. Presented here is soft molding method with a highly accurate rigiflex mold for multistep nanopattern fabrication with a high feature density. More interestingly, the rigiflex mold softens dramatically upon reaching a temperature of 50 C whereas it is harder than the usual PDMS mold (Yoo et al. 2004).

Figure II-5 illustrates schematically the soft molding process. First, a polyelectrolyte multilayer (polydiallydimethyl ammonium chloride/sulfonated polystyrene (SPS) layer) as an adhesion promotion layer was formed onto a substrate via an alternating adsorption process. The warm rigiflex mold at 50-60 C is placed onto an SPS film immediately after the film is spin-coated onto an adhestion promotion layer from a 20 wt% SPS aqueous solution as a transfer layer.

At the softening temperature, the mold becomes conformal with the underlying polymer film that is to be molded. At this point, the spin-coated film is still wet with residual water (25-35 wt% SPS with films). The rigiflex mold is then pressed lightly onto the substrate of the SPS film at a pressure of less than 1 Ncm-2, and the substrate is allowed to remain in contact undisturbed for a period of time (20 min) for solidification on a hot plate at 50-60 C, during which time the solvent in the molded structure is absorbed onto the mold. the rigiflex mold is then peeled off the substrate while hot. In this soft molding process, the solvent absorption of the rigiflex mold is an important factor. According to this experiment, the rigiflex mold made of polyurethane (PU) chemistry can absorb 1% of its weight in water at 50 C. the selection of 20 wt% aqueous solution of SPS as transfer layer was advantageous for the use of the rigiflex mold because the PU acrylate-based rigiflex mold is permeable to water vapor, providing for absorption and evaporation of the residual solvent under the mold conditions. A comparison of the rigiflex mold with the transferred nanopattern reveals that the pattern of the mold is well replicated in the SPS layer that is transferred to the substrate (Rogers and Lee 2009).

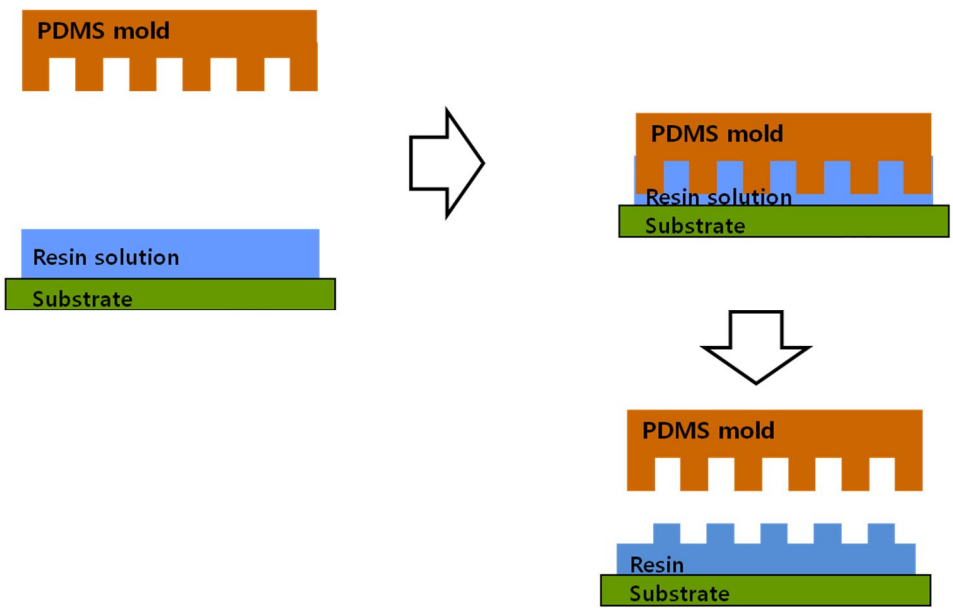

Figure II-5. An illustration of the procedure for fabricating a replica on a substrate from soft molding.

II.3.3.2 Capillary force lithography applications

Recently, by combining essential features of nanoimprint and capillarity, the capillary force lithography (CFL) was developed for fabricating polymeric micro/nanostructures over large areas (Suh et al. 2001, Suh and Lee 2002, Yoon et al. 2006). In this method, one directly places a patterned elastomeric mold onto a spin-coated thermoplastic resin on a substrate and then produces a negative replica of the mold by raising the temperature above the resin`s glass transition termperature after solvent evaporation (temperature-induced capillarity), which contrasts the direct soft molding prior to solvent evaporation (solvent –induced capillarity). There has always been a prerequisite to the mold that is used for CFL, which is the permeability of the mold with respect to gas. If the mold is impermeable, the air trapped in the voids between the mold and the substrate surface gets compressed as the voids get filled by capillary action, which prevents the capillary rise.

In this section, the mechanism of CFL was investigated. The driving force for the capillary rise in a capillary of radius r is the Laplace pressure P_L that is given by

$$P_L = \frac{2\gamma \cos\theta}{r} \qquad 1)$$

Where γ is the surface tension and θ is the contact angle that the material filling up the pore makes with the capillary (Suh et al. 2001, Suh and Lee 2002). If the

capillary rise takes place at atmospheric pressure and the capillary rise is to a height of z in a capillary tube of length Z, the pressure of the trapped air in the tube Pa is given by Z/(Z-z) or 1/(1- Z_m) where Z_m is z/Z. the capillary rise will cease when P_a equals the Laplace pressure. Therefore, the normalized height Z_m to which the material of interest rises at atmospheric pressure (1 bar) is given by

$$Z_m = 1 - \frac{1}{P_L} \qquad 2)$$

where P_L is in bar unit. The geometric factor r/2 in equation x is the ratio of the exposed surface area to the circumference that is in contact with the wall. When a channel infinitely long is involved, the geometric factor becomes L./2 where L is the channel width (Khang and Lee 2004b). Therefore, equation 2 applies to the channel if r is replaced by L. As the relationship shows, there is no capillary rise taking place if the Laplace pressure is less than 1 bar. On the other hand, equation 2 tells us that the Laplace pressure increases inversely with the capillary radius or equivalently with the feature size of a pattern and that as the radius decreases, the pressure should exceed 1 bar. In fact, the Laplace pressure can far exceed atmospheric pressure if the radius or feature size is sufficiently small, ensuring that CFL should be possible with impermeable mold. When an impermeable hard mold is pressed against a hard substrate as in NIL (nano imprint lithography), however, the pressure needed for the intimate contact all over the pressed areas is so high that it far exceeds the Laplace pressure because of the inherent roughness present on the mold as well as on the substrate. Therefore, the capillary force is still

inconsequential. Accordingly, we used the rigiflex mold for resolving an intimate contact problem, which is rigid enough for fine patterning and yet flexible when it is made in a film form. In fact, this impermeable rigiflex mold has been shown to be rigid enough to be used for NIL (Lai et al. 2009).

For system under consideration where the CFL was carried out at 150 C with polystyrene (PS), the capillary pressure can be calculated from equation 2 with $\gamma_{PS\text{-}air} = 40$ mNm^{-1} and contact angle ($\theta = 56.6$ °) of PS with the rigiflex mold as a function of the pattern size, resulting in exceeding the atmospheric pressure for the feature size smaller than about 440 nm. Therefore, the capillary rise should ensue at atmospheric pressure of the feature size smaller than 440 nm.

The patterning result by CFL with the rigiflex mold is compared according to feature size in Figure II-5. As can be seen in Figure II-5, where the pattern of large feature size was used (bottom diameter of 6 μm and height of 10 μm), little capillary rise should have occurred because the diameter is not small enough for sufficient capillary pressure. In constrast, it can be seen from Figure II-5 that the PS pattern formed has a height of approximately 150 nm where the master shown in fig x was used, which is a 80 nm line/ 60 nm space pattern made of aluminum. For the 80 nm wide channel in the rigiflex mold, the corresponding capillary pressure is about 5.5 bar. According to equation 20.3 capillary rises should be 139 nm since the channel depth is 170 nm. This calculated capillary rise compares with the experimental result of about 150 nm in Figure II-5.

A simple capillary kinetic model has also been presented to describe the

capillary rise of polymer melt into a less permeable mold. the kinetic model predicts that the capillary rise is linearly proportional to the time for less permeable molds, which has been verified using rigiflex molds with poly(ethylene terephthalate) (PET) film as a supporting layer. It has been shown that for a given mold geometry, the height of nanostructure is tunable by changing the annealing time. Also, the tip shape can be rounded or dimpled depending on the temperature as a result of reflows of polymer melt.

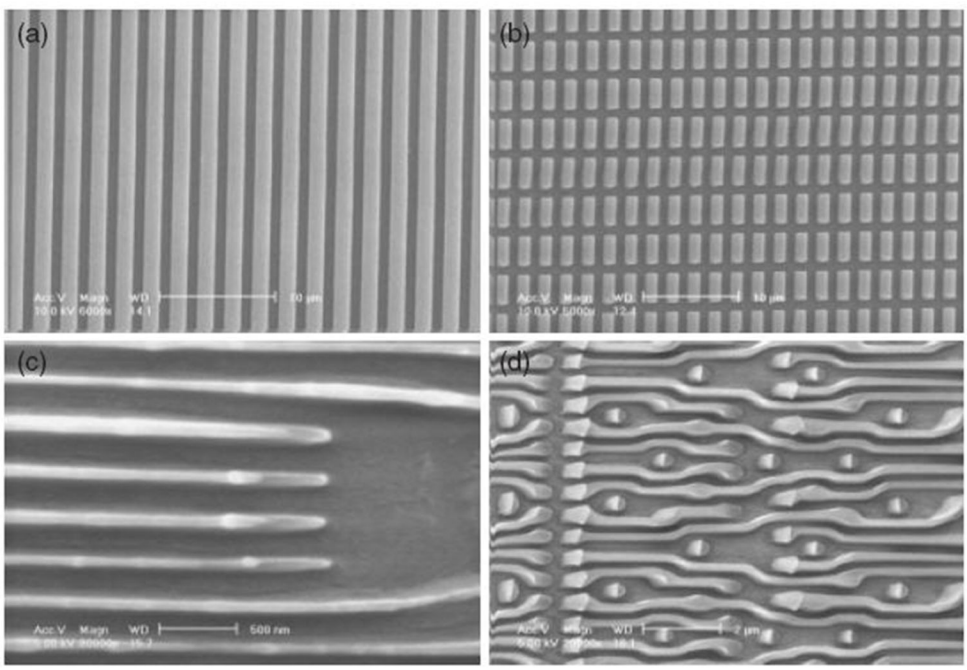

Figure II-6. SEM images of (a) master pattern (75 nm lines separated by 75 nm), (b) nonsist of square arrays (80 nm), (c) master pattern, 80 nm line/270-nm space pattern, and (d) replica mold (PVA) (Suh et al. 2001)

II.3.3.3 Rapid flash patterning for residue-free patterning

The rapid flash patterning (RFP) allows for the exposure of the substrate surface (Yoon et al. 2004). Although many techniques are available for large area, general purpose patterning, there are a number of aspects yet to be resolved such as the speed, which the patterning can be accomplished, and exposure of the substrate surface in the course of the patterning. Sub- 100 nm structure can be fabricated in tens of seconds with and aspect ratio much larger than unity by the general purpose patterning method introduced here. Unlike other unconventional methods, the substrate surface can be made exposed and the resulting pattern height is sufficiently high for subsequent etching of the substrate. A rigiflex mold and a rapid flash heating by an infrared lamp are the main ingredients of the technique.

The rapid flash patterning (RFP) method is shown schematically in Figure II-6. A thin rigiflex mold is placed on the polymer layer that has been spin-coated ontoa substrate and dried. To assure a uniform pressure distribution when pressed, a PDMS block is placed on the mold followed by a glass plate, onto which pressure is applied, typically 3-4 bars. In the pressed state, a halogen lamp in infrared (IR) range is flashed for a short period of time, typically 60 s with a 500 W lamp, but 10 s with 10 KW lamp array. The temperature reached is typically around 260 °C After a few minutes of cooling, the pressure is relieved, followed by removal of the rigiflex mold, leaving behind a patterned polymer layer on the substrate.

Shown in Figure II-7 is a sub-100 nm pattern formed by RFP on poly(vinylalcohol) (PVA) surface with a 500 W IR lamp. The cross-sectional SEM

image of the line and space pattern in Figure II-7 is shown in Figure II-7 for the 80 nm wide lines, the patterned line height is 440 nm, which gives an aspect ratio in excess of 5. One-step reactive ion etching was carried out with the polymer pattern formed in Figure II-7 to etch into the underlying silicon layer. The plasma –etchant gas was CF_4 at a rate of 15 sccm and a total pressure of 5.4 mTorr with a power of 300 W. the measured etch rate was 5 and 10 nms-1 for the silicon and the PVA polymer, respectively. The result is shown in Figure II-7. even though the etch rate of the poymer was twice the rate of silicon, the silicon was etched to a 200 nm depth because of the high aspect ratio of the patterned polymer.

The essence of RFP lies in the use of a flexible, rubbery mold. When a hard mold is used as in the ultrafast technique, the substrate surface does not get exposure because the dewetting connot take place due to the rigidity of the hard mold. Furthermore, any possible local contact of the hard mold with the underlying hard substrate, even if it is possible, would lead to breakage of one of the hard plates. The rigiflex mold used for RFP has a Young`s modulus of 0.3 GPa, compared to 107 GPa for silicon, that is high enough for fine patterning technique that has been developed to meet some of the patterning requirements for large-area applications.

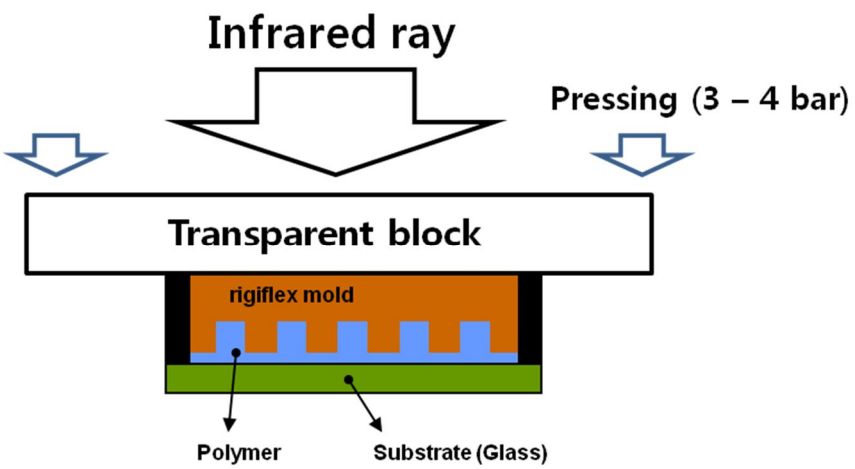

Figure II-7. Schematic illustration for the rapid flash patterning method.

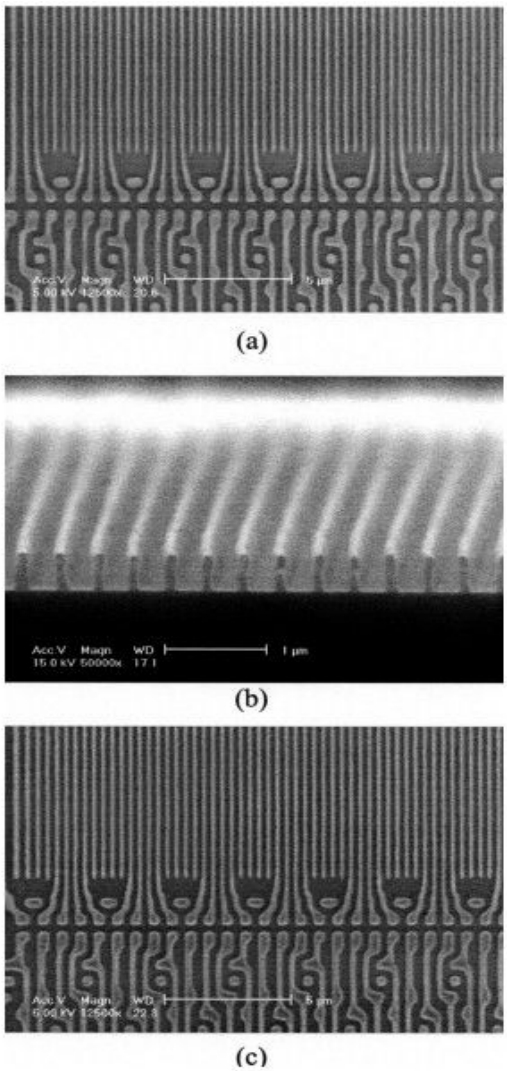

Figure II-8. PVA pattern formed by RFP in which substrate surface is exposed (80 nm wide lines and 270 nm space between the lines). (a) SEM image of patterned polymer. (b) cross-sectional SEM image of the line in (a). (c) Silicon pattern etched wih polymer resist of (a).

II.3.3.4 Nano imprint and micro-contact printing

Nano imprint lithography is a technique to generate nanostructures by mechanically pressing a hard mold with surface relief features into a thin thermoplastic polymer film that is then heated above the glass transition temperature (Tg) of the polymer. Micro-contact printing as one of the typical soft lithography is a technique to define a pattern by transferring a molecular ink from a patterned elastomeric mold onto substrate by conformal contact (Li et al. 2003, Dai et al. 2007, Takulapalli et al. 2011). In order to define the pattern successfully, the material of mold plays a major role during two processes (Xia and Whitesides 1995). Thus, in this section, the use of the mold material for two contrasting lithographic techniques will be described.

Physical patterning of imprinting that is usually carried out with a hard mold and chemical patterning of micro-contact printing that is usually carried out with an elastomeric soft mold. For the two contrasting methods, the mechanical properties can be tuned to each application by choosing a cross-linking modulator that can modulate the chemical structure of the UV-curable mold material (Xia et al. 1996, Suh et al. 2003).

A radiation-curable modulator plays a key role in preparing the mold material. Mixing the monomer modulator with the prepolymer, which possess trifunctionality in the form of cycloaliphatic and high molecular structure for a balance between rigidity and flexibility, results in a reduction of viscosity that allows the mixture to fill very fine structures of sub -100 nm channels or holes.

More importantly, the modulator allows on to change the chain length or cross-linking density, which further leads to a modification in the mechanical properties (Tan et al. 1998, Lim et al. 2011, Lim et al. 2012, Park et al. 2012)

.

II.3. Patterned membranes

II.3.1.History of patterned membranes

The development of patterned membrane was started with convergence of soft lithography and phase inversion method. The converged technique is phase separation micro molding. (PSμm). Laura et al firstly introduced the PSμm method in 2005 and emphasized its possibility of application to diverse engineering field. After the first introduction about the PSμm method, wesseling group firstly developed patterned polymeric films using PSμm method (Peters et al. 2008). A polymer solution is applied and contained between two substrates, of which at least one is a patterned PDMS mold. The ensemble is then put in an atmosphere containing water vapor, which diffuses through the PDMS. The absorption of water into the polymer solution causes the precipitation (phase separation) of the polymer while in contact with the microstructured molds. The thickness of the PDMS slab can be exploited to tune the water vapor transport and hence the phase separation kinetics and resulting polymer morphology. Removal of excess polymer solution from between two PDMS slabs, followed by vapor induced phase separation, can also result in micro-perforated polymer films with great control over the dimensions.

Although the first patterned membrane was developed by Bikel et al (Bikel et al. 2009), it revealed critical problem of PSμm method. It is that the phase separation is always induced from the non-patterned side (i.e., the side that is not in

contact with the mold and is open to the coagulating agents). The coagulation front moves through the film, often creating a hierarchal pore size gradient. As the nonsolvent diffuses into the polymer solution, it drags along solvent with it. This creates a variation in local concentrations of nonsolvent across the membrane, leading to pore size differences. The pore size decreases toward the side originally in contact with the coagulation bath. Often, a dense skin is formed on this interface. As a result, the dense layer of a membrane is located on the unstructured side.

In 2012, Won et al reported the patterned membrane prepared by modified immersion precipitation method (Won et al. 2012). It was developed to relieve the formation of dense layer at the solvent−nonsolvent interface, that is, the opposite side of the patterned surface. Also they prepared diverse patterned membranes, such as pyramid-, prism-, and embossing-patterned membranes and compared with a flat membrane in terms of morphology, permeability, and biofouling. At around the same time, Culfaz et al. prepared a patterned hollow fiber membrane by a patterned spinnerette and observed that the patterned membrane exhibited higher water flux than that of the conventional hollow fiber membrane (Culfaz et al. 2011a, Culfaz et al. 2011b, Culfaz et al. 2010, Culfaz et al. 2011c). They also found that the fouling resistances of structured fibers were better than those of normal hollow fibers under specific conditions.

Recently, in addition to the PSμm method, novel approaches to prepare membrane using lithographic method. Choi et al. prepared micro- and submicron-sieve membranes with uniform, non-tortuous pores using a soft-lithographic

technique (Choi et al. 2013). Different with the PSμm method, nano imprint lithography was converged with membrane preparation process. The pore was directly controlled by the pillar of master mold thus the precisely controlled pore size, spatial distribution and non-tortuous quality, the membrane flux per surface porosity was shown to be greatly enhanced in comparison with conventional membranes with a tortuous pore structure. Furthermore, the solventless UV-curable polyurethane acrylate (PUA), employed as the membrane material, has lower surface energy leading to much better anti-biofouling performance than other commercial membrane materials. The soft-lithographic technique and UV-curable polyurethane acrylate (PUA) introduced here would open a horizon to a new generation of membranes with anti-fouling capability (Choi et al. 2004).

II.3.2. Phase separation micro molding process

A schematic representation of the PSμm is illustrated in Figure II-8. In PSμm a polymer solution is applied on a mold, having a micrometer-sized relief structure on the surface. The application of the solution on the mold is performed normally by casting. When the thickness of the layer of polymer solution is a critical parameter, a set-up was used in which the height of the casting knife can be adjusted by micrometer positioners, ensuring accuracy of the film thickness. The polymer solution is solidified by phase inversion and during the solidification assimilates the profile on the mold. Depending on the composition of the solution and the non-solvent, the resulting polymer film may exhibit an intrinsic porosity after the phase inversion. Phase inversion on a mold can therefore result in porosity within a patterned polymer product.

The porosity of both the surface (patterned surface and non-patterned surface) and the inner surface is completely determined by the conditions under which the phase inversion takes place, e.g. the composition of the polymer solution and the non-solvent. The porosity can therefore be tailored by choosing the right composition of the solution and non-solvent. As a rule of thumb a higher polymer concentration and a higher molecular weight of the polymer result in a denser polymer film. The pore morphology strongly depends on the kinetics of the exchange between solvent and non-solvent as well. A slower demixing process in general results in a denser polymer. The demixing is delayed for instance by choice of a non-solvent having low miscibility with the solvent. Also, the use of ether

polymeric or low molecular weight additives can slow down the demixing process. Another option to influence the exchange of solvent and non-solvent is by either adding a small amount of non-solvent to the solution, or by adding solvent to the non-solvent.

During a relatively fast demixing process macrovoids can form: large finger-like cavities below the surface of the film. Although macrovoids in general do not appear at the surface, they locally disturb the mechanical properties and can therefore lead to defects in the microstructure on the surface of the polymer film. Macrovoids in a microstructured polymer are depicted in fig x. formation of macrovoids can be prevented by adaptation of the recipes, for example by including certain additives in the solution. Another method that may prevent the formation of macrovoids is to precede the vapor induced phase inversion. The polymer solution on the mold is first exposed to the environment of nitrogen, saturated with non-solvent vapor. The non-solvent vapor dissolves into the polymer solution, causing the pahse inversion to set in as can be seen from the turbidity of the film. The non-volatile solvent, however, remains in the solution. Subsequently the mold and the polymer film are immersed in a non-solvent bath, which extracts the remaining solvent from the film and finalizes the phase inversion. When the non-solvent induced phase inversion is combined with such a vapor step, it is observed that the homogeneous pore distribution, reduced skin formation, and absence of macrovoids. A typical example of preventing macrovoids formation by additional vapor step is given in Figure II-8.

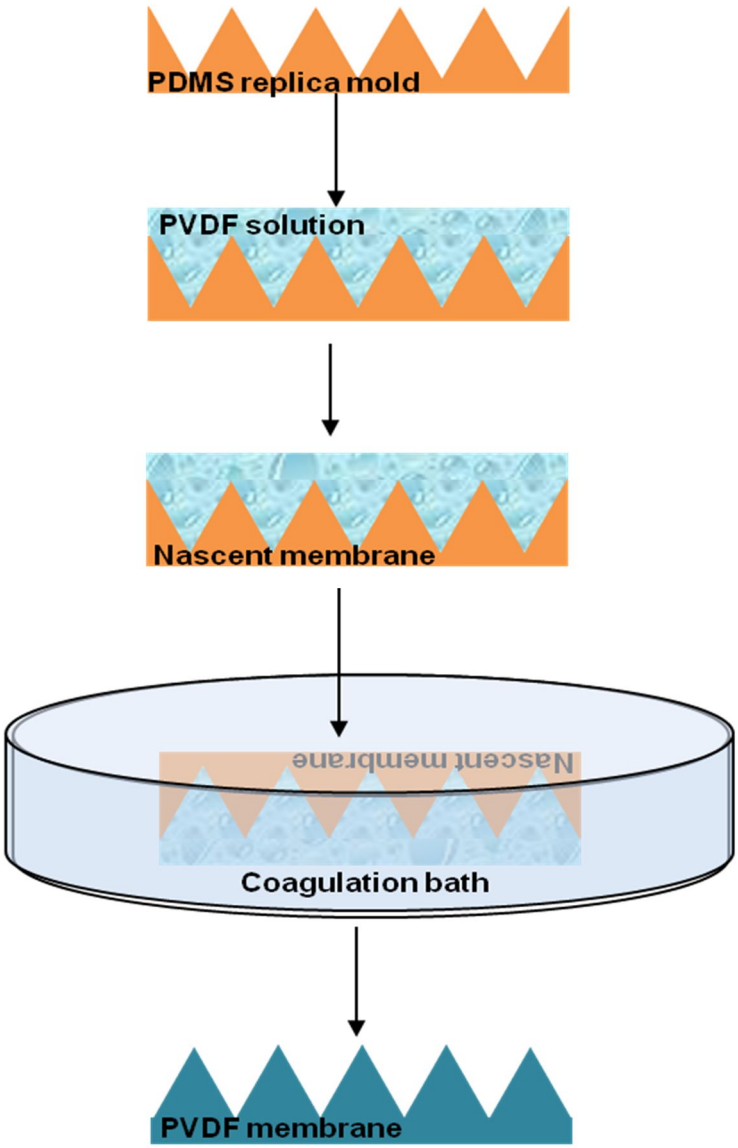

Figure II-9. Schematic diagrams of PSμm process

.

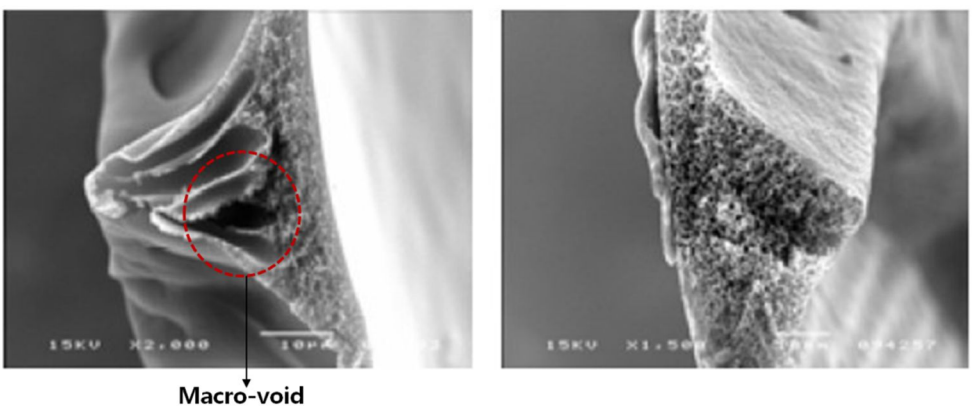

Figure II-10. Cross-sectional SEM images of patterned membrane (left) macro-void was formed within the patterns, (right) uniform pore structures

II.4. Membrane Bioreactor (MBR)

II.4.1.MBR for Advanced Wastewater Treatment

The microorganism involved either membrane bioreactor (MBR) technology combines the biological degradation process by activated sludge with a direct solid-liquid separation by membrane filtration, By using micro or ultrafiltration membrane technology (with pore size ranging from 0.05 to 0.4 μm), MBR systems allow the complete physical retentation of bacterial flocs and virtually all suspended solids within the bioreactor. As illustrated in Figure II-9, MBRs are similar to conventional activated sludge systems (CASs) with the exception that the biomass (i.e., microorganisms) responsible for removing the contaminants of concern are retained within the bioreactor component of the system using membranes (Figure II-9b, c) rather than secondary clarifiers (

Figure II-11. Schematic diagrams of bioreactor processes a). However, the MBR has many advantages over conventional wastewater treatment processes. These include high effluent quality, good disinfection capability, higher volumetric loading and less sludge production. As a result, the MBR process has now become an attractive option for the treatment and reuse of industrial and municipal waste waters. However, the MBR filtration performance inevitably decreased with filtration time. This is due to the deposition of soluble and particulate materials onto and into the membrane, attributed to the interactions between activated sludge components and the membrane. Thus this major limitation has been under

investigation since the early MBRs, and remains one of the most challenging issues facing further MBR development.

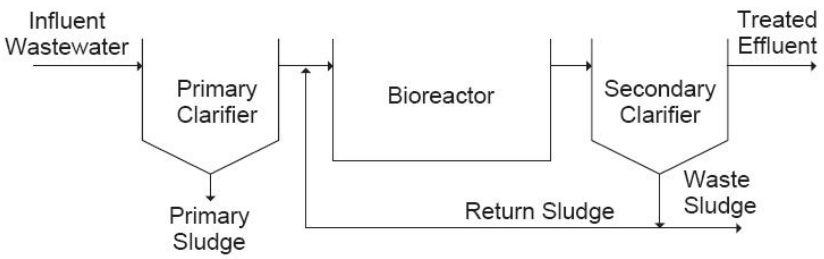

a) Conventional activated sludge system

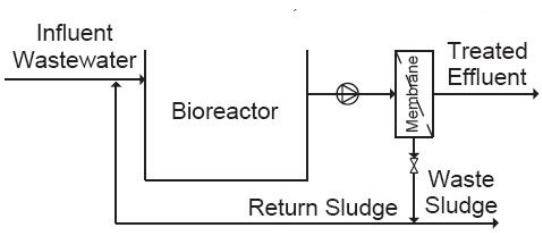

b) External Membrane MBR

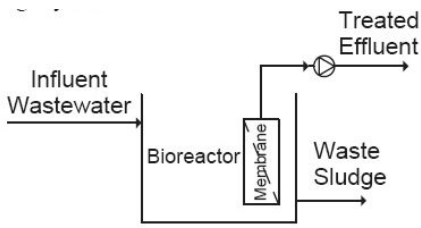

c) Submerged Membrane MBR

Figure II-11. Schematic diagrams of bioreactor processes (Escobar and Schäfer 2010).

II.4.2. MBR History

The MBR process was introduced by the late 1960s, as soon as commercial scale ultratiltration (UF) and microfiltration (MF) membranes were available. The original process was introduced by Dorr-Olivier Inc. and combined the use of an activated sludge bioreactor with a crossflow membrane filtration loop. The flat sheet membranes used in this process were polymeric and featured pore size raging from 0.003 to 0.01 μm (Enegess et al. 2003). Although the idea of replacing the settling tank of the conventional activated sludge process was attractive, it was difficult to justify the use of such a process because of the high cost of membranes, low economic value to fouling. As a result, the focus was on the attainment of high fluxes, and it was therefore necessary to pump the mixed liquor suspended solids (MLSS) at high crossflow velocity at significant energy penalty of the order 10kWh/ m3 product) to reduce fouling. Due to the poor economics of the first generation MBRs, they only found applications in niche areas with special needs like isolated trailer parks or ski resorts for examples. The breakthrough for the MBR came in 1989 with the idea of Yamamto et al. to submerge the membranes in the bioreactor (Yamamoto et al. 1989). Until then, MBRs were designed with the separation device located external to the reactor and relied on high transmembrane pressure (TMP) to maintain filtration

In 1997, the first Kubota municipal wastewater treatment works installed outside Japan was at Porlock in the United Kingdom. And the first Zenon membrane-based plant of similar size installed outside of the USA was the Veolia

Biosep® plant at Perthes en Gatinais in France in 1999. Both these plants have a peak flow capacity just below 2 mega liter per day (MLD), and represent landmark plants in the development and implementation of immersed MBR technology.

II.4.3.Trends in MBR: Market and Research

II.1.3.1. World Market

Since first been developed at 1960s, the MBR has been widely used in water reuse systems in building, industry, sanitary treatment and municipal wastewater treatment. In commercial use for little more than a decade, MBR is beginning to realize its market potential in wastewater treatment and water recycling for industrial, municipal, in-building and marine use. Consequently the MBR has emerged as a key technology for present and future wastewater treatment and reuse schemes.

A recent market survey estimates for the global market expenditure on MBR to $280 million in 2007. Also it is rising at a compound annual growth rate (CAGR) of 13.7%, which is faster than the total market for wastewater treatment plant of 7.3% CAGR (Sze Chai Kwok 2010). In addition, more than 4,400 MBR plants have been installed worldwide by the end of 2009 (Judd and Judd 2011).

II.1.3.2. Research: Membrane Fouling

The research trend in MBR technology was reviewed by the data on the number of articles published since year 1995. As shown in Figure II-10, number of published papers increased dramatically since year 2005 in similar way with global market value, which suggests growing acceptance of MBR technology and escalating technical demand to overcome the perceived drawbacks of MBR such as its complex and small scale nature, high costs and operator skill requirements.

The performance of MBR process is mainly deteriorated by the membrane fouling which is the occlusion or blocking of membrane pores at the surface of the membrane. This membrane fouling causes severe operation problems of flux decline, short membrane life-span, and increases of energy consumption and therefore, has been regarded as a main obstacle restricting the development of MBR technology. As clearly shown in Figure II-10, about 50% of MBR researches were dedicated to the topic of fouling including investigation of the mechanism and development of the control techniques.

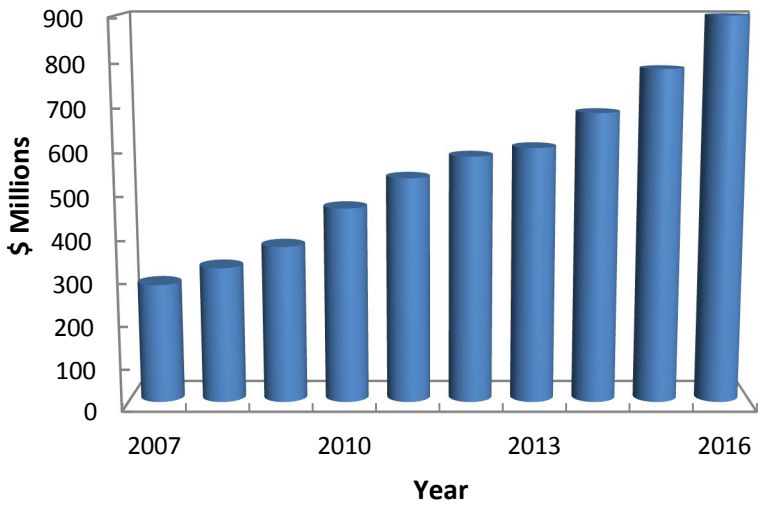

(a)

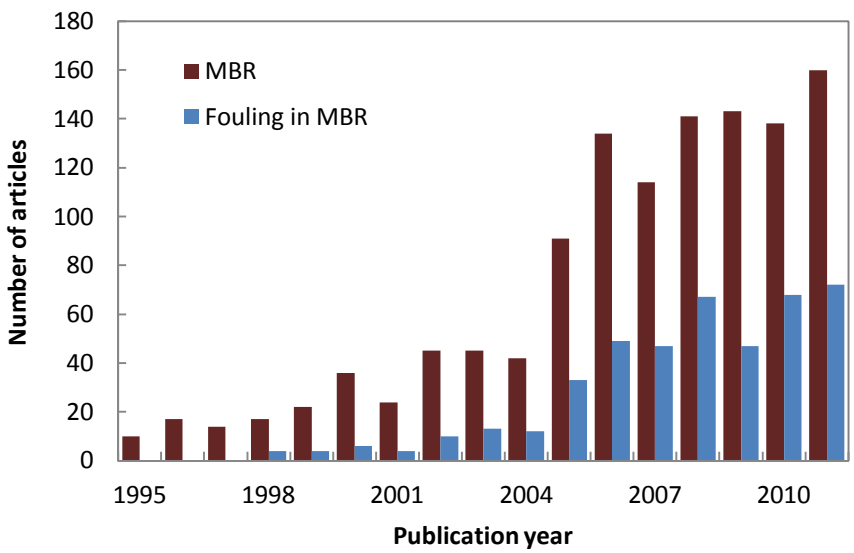

(b)

Figure II-12. Market and research trends in MBR. (a) global market value and (Sze Chai Kwok 2010) (b) number of research articles published since 1995 (Source: ISI)

II.4.4.Advantage and disadvantage of MBR

II.1.3.2. Advantages of MBR

♦ Compared to conventional wastewater treatment technologies, sludge retention time (SRT) of membrane bioreactor (MBR) is independent of hydraulic retention time (HRT). Therefore a very long SRT can be maintained resulting in complete retention of slowly growing microorganisms, such as nitrifying bacteria, in the system. Also, it is possible to maintain high concentration of microorganisms in bioreactors while keeping the microorganisms dispersed a long as desired and as a result reactor volume will be less.

♦ Since suspended solids are totally eliminated through membrane separation, the sttleability of the sludge, which is the problem in conventional activated sludge, has absolutely no effect on the quality of the treated effluent. Consequently the system is easy to operate and maintatin

♦ Removal of bacteria and viruses can be expected, so the disinfection process is ecologically sound.

♦MBR effluent has very low biological oxygen demand (BOD) (Less than 5 ppm), is virtually free of suspended solids. Therefore, treated wastewater is suitable for sending to a reverse osmosis (RO) system for dissolved salts removal, or for recycling and reuse without further treatment.

♦ Because all the process equipments can be tightly closed, the MBR system does not need large amount of ground.

II.1.3.3.Disadvantages of MBR

♦ The life time of membrane has not been firmly established. Although the apparent widespread acceptance of the process in Japan indicates the membranes have some degree of long-term reliability, a literature review did not find quantification of the life span in terms of years or volume of waste treated.

♦ Fouling results from the accumulation and attachment of particulate and dissolved material at the surface of the membrane, which causes a significant resistance to filtration. Additionally, the presence of stringy material such as hair or rags would significantly reduce membrane operation.

♦ In the separate-stage configuration, the circulation pumps that feed the membranes can consume considerable energy. This can lead to relatively high operating costs and may limit its applications.

♦ Last, both MBR configurations periodically will require some form of chemical membrane cleaning. This can be accomplished with chlorine solution, or sometimes by immersion in an acid bath. However, the additional chemical storge and handling requirements created may be undesirable at some facilities.

♦ Almost the process equipments need to high capital and operating costs such as aeration is too high.

Chapter III

Designing of preparation steps for diverse patterned membrane

III.1. Introduction

As was clearly shown in the literature review section, membrane fouling remains a critical factor limiting the widespread use of membrane processes in water and wastewater treatment. In order to mitigate membrane fouling, we introduced a patterned morphology on the membrane surface using a lithographic method. This modified immersion precipitation method was developed to prepare the diverse patterned membrane. With aid of the modified phase inversion method, diverse patterned membranes, such as pyramid- and prism-patterned membranes, were prepared and compared with a flat membrane in terms of morphology. Also, the relations between the fidelity of patterned membrane and preparation conditions were investigated.

III.2. Experimental Section

III.2.1. Preparation of PDMS replica mold

We used two types of master pattern (pyramid, prism) that were fabricated by photolithography in a nano-patterning organic devices laboratory in Seoul National University. Detailed size and shape of the patterns was illustrated in Figure III-1. As the photo-resist (PR) masters were swelled easily in organic solvents, however, they were not suitable for use in the immersion precipitation method by which the patterned membrane was to be prepared. Consequently, PDMS replica molds were used as substrates in the preparation of patterned membranes. PDMS was chosen as a replica material because of its advantages, such as low surface energy and inertness to various organic solvents. The PDMS mold was prepared as follows: the PDMS was mixed with the curing agent in a ratio of 10:1. The mixture was poured onto the photoresist master mold, and was then cured at 60 ºC for 2 h. The replica mold was obtained by peeling off the cured mixture.

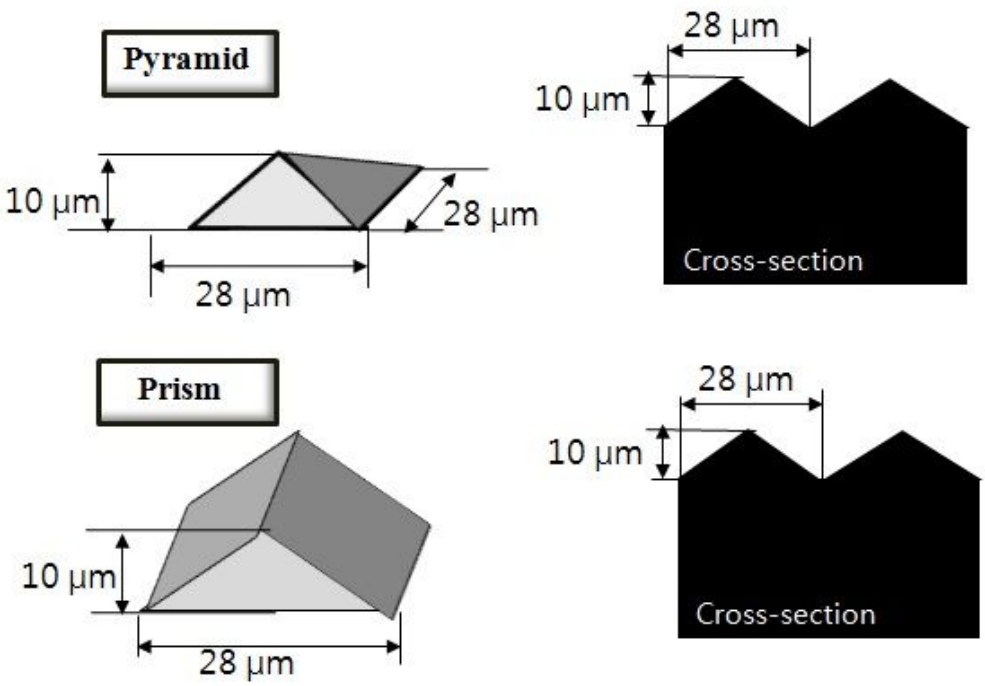

Figure III-2 Characteristics of two types of patterned membranes.

III.2.2. Membrane materials

Polyvinylidene fluoride (PVDF), dimethyl-formamide (DMF) and acetone were purchased from Sigma Aldrich Korea and used without further purification, while Polydimethylsiloxane (PDMS, Sylgard 184) were obtained from Dow Corning Corporation. Deionized water was used for the precipitation bath. The non-woven fabric of a polysulfone ultrafiltration membrane (Woongjin Chemical Co. Ltd., Korea) was used as a substrate for the preparation of the patterned PVDF membrane.

III.2.3. Membrane preparation

A casting PVDF solution was prepared as follows: a PVDF pellet was dissolved in DMF at 60 °C for 6 hr and acetone was then added at room temperature. The mixed solution of PVDF, DMF and acetone was stirred overnight for complete mixing. A schematic diagram of the membrane preparation process is depicted in Figure Ⅲ-2. Usually, in the conventional immersion precipitation method (Figure Ⅲ-2a), the PVDF solution is poured on the substrate (non-woven fabric), spread by a casting knife, and then coagulated in a precipitation bath. However, we had to develop a modified immersion precipitation method for the preparation of the patterned membrane (Figure Ⅲ-2b): the casting solution was poured on the patterned PDMS replica mold and uniformly doped with the casting knife. Immediately after the casting, the fabric was placed on top of the casting solution (the nascent membrane). The nascent membrane, together with the fabric and PDMS replica, was dipped into the precipitation bath and coagulated for 6–10 hr. The patterned membrane with the fabric as a support layer was then released from the PDMS replica mold and stored in a bath filled with de-ionized water.

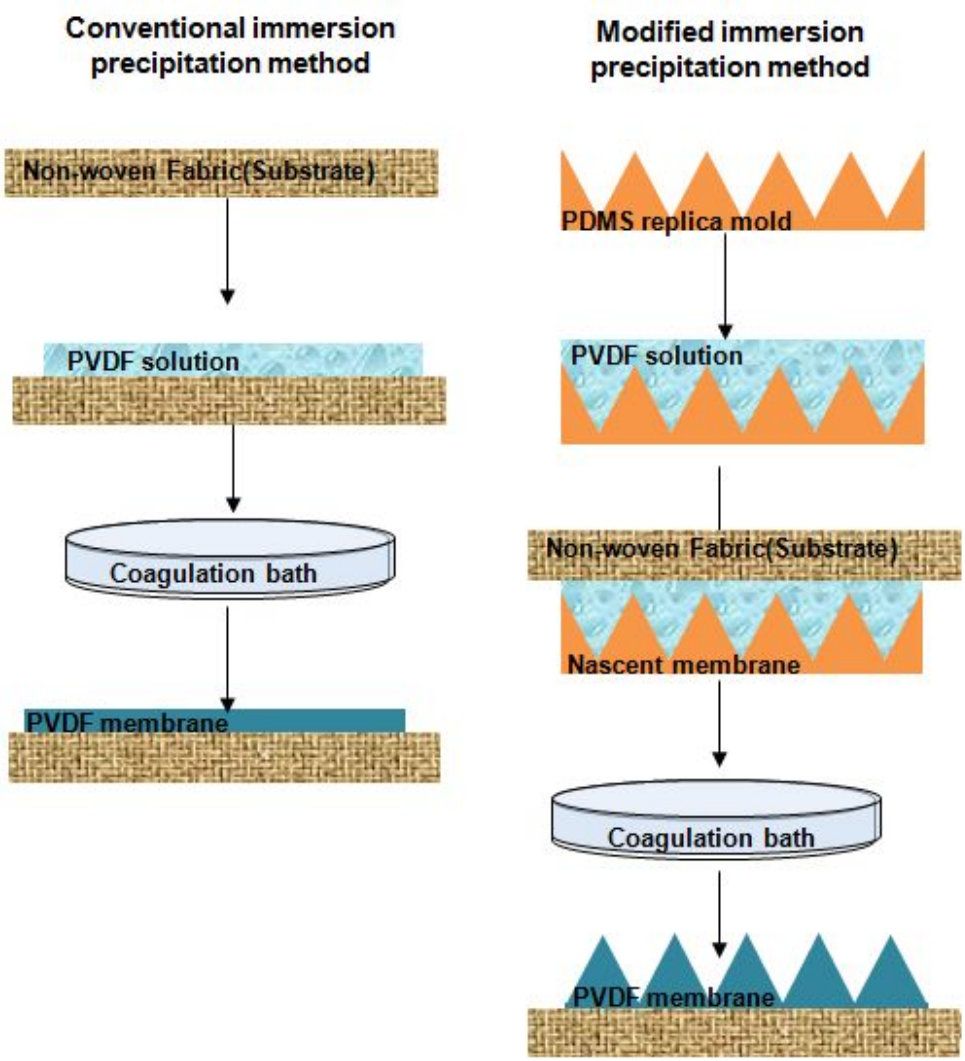

Figure III-2. Schematics of a) a conventional immersion precipitation method, and b) a modified immersion precipitation method.

III.2.4. Calculation of pattern fidelity

The width and height of the prism-patterned master mold were 48-50 μm and 18-21 μm, respectively. Bessonov et al. defined pattern fidelity by the ratio of the pattern length (width) in the master mold to that of the replica mold (Bessonov et al. 2011). This definition may be applicable to a one dimensional pattern consisting of lines and spaces, because only the pattern lengths of the master mold and replica mold are compared. However, this does not seem to be suitable to the prism pattern in this study because the width and height of prism should be considered simultaneously. Thus, we introduced "Area Fidelity", which represents the pattern fidelity based on pattern area instead of pattern length. In order to describe the fidelity of the prism pattern in more detail, however, we also used "Width Fidelity" and "Height Fidelity" in addition to "Area Fidelity":

$$\text{"Area Fidelity"} = \frac{\text{(Area of pattern in a patterned membrane)}}{\text{(Area of pattern in a replicated module)}}$$

$$\text{"Width Fidelity"} = \frac{\text{(Width of pattern in a patterned membrane)}}{\text{(Width of pattern in a replicated module)}}$$

$$\text{"Height Fidelity"} = \frac{\text{(Height of pattern in a patterned membrane)}}{\text{(Height of pattern in a replicated module)}}$$

III.3. Results and Discussion

III.3.1. Preparation steps of patterned membranes.

The phase inversion of a polymer solution with nonsolvent is usually divided in two ways, depending on precipitation methods. The first is the precipitation from the vapor phase, in which the phase separation of a polymer solution is induced by the penetration of nonsolvent (water) vapor into the polymer solution. The second is the immersion precipitation method, in which a polymer solution is cast on the substrate and subsequently immersed in a nonsolvent bath. At first, we adopted both these two conventional methods to prepare prism-patterned membranes (Reuvers and Smolders 1987, Reuvers et al. 1987).

Firstly, the phase inversion of the nascent membrane (i.e., PVDF solution) was performed by drying in the air at 22% of humidity for 24 h at room temperature (vandeWitte et al. 1996a). The polymer solution was changed into a dense film with a prism-patterned structure (Figure III-3a), which could not be regarded as a porous membrane; this was because the polymer solutions had preceded slow liquid–liquid demixing in a conventional air drying method.

Secondly, the nascent membrane was directly immersed in a coagulation bath. In this case, the prism-patterned membrane was much more porous in comparison to the former method (Figure III-3b). The structural difference

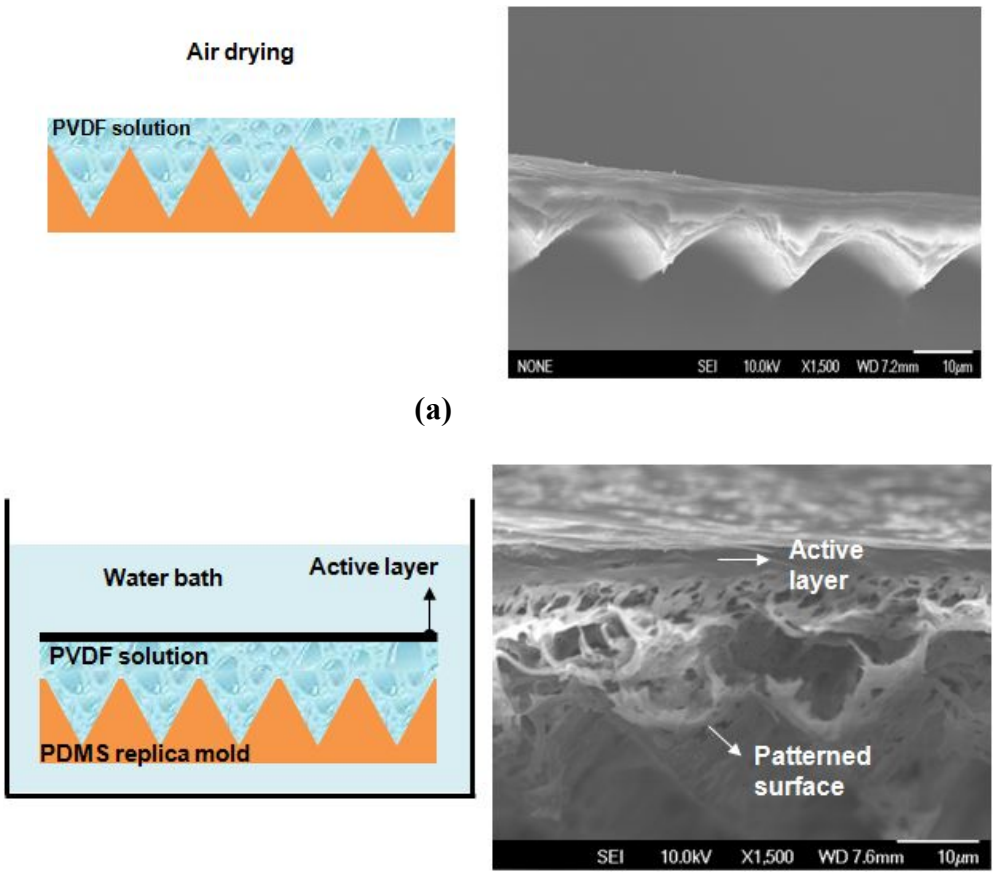

Figure III-3. SEM image and location of the active layer of a prism-patterned membrane prepared by (a) a conventional air drying method, and (b) a conventional immersion precipitation method.

Between the two patterned membranes was attributed to a difference in the demixing rate between water (or vapor) and nonsolvent. Reuvers et al. claimed that the mass transfer processes associated with most membrane forming systems can be divided into two categories: delayed demixing and instantaneous demixing (Reuvers and Smolders 1987, Reuvers et al. 1987). Delayed demixing produces a membrane with a dense sponge-like structure due to slower permeation of water into the polymer solution. In contrast, instantaneous demixing results in a membrane with a porous finger-like structure. In our case, the cross-sectional SEM micrograph illustrated in Figure III-3b shows the active layer was located at the opposite side of the prism-patterned surface and there were many macro-voids inside the membrane, indicating that it was prepared under instantaneous demixing. Nevertheless, it is worth noting that the second method produced a patterned membrane with an active layer on the opposite side of the patterned surface, although the preference was that the active layer of the patterned membrane would be on the same side of the patterned surface (vandeWitte et al. 1996a, Tsai and Torkelson 1990).

In the conventional immersion precipitation method, the starting point of the demixing process governs the location of the active layer, which is at the solution/nonsolvent interface. Consequently, it would be impossible to prepare patterned membranes such as these with the active layer on the patterned surface using this method. One of the ways to overcome this barrier might be to change the solution/nonsolvent interface at the patterned surface. However, this was found to

be nearly impossible because the patterned surface was blocked by the PDMS mold.

As a result, the modified immersion precipitation method was conceived, taking into account the transfer of substrate (non-woven fabric) from the bottom (Figure III-2a) to the top (Figure III-2b) of the nascent membrane. In other words, the nascent membrane was covered with substrate prior to its immersion in the precipitation bath, as shown in Figure III-4. The modified method gave rise to a patterned membrane in which a porous layer with macrovoids, instead of a dense active layer, was formed at the solvent/nonsolvent interfacial surface.

To explain the formation of macro-pores, Termonia et al. suggested that non-solvent penetration initiates the growth of macrovoids through defects in the active layer (Termonia 1995). In this study, the irregular pores in the substrate (non-woven fabric) might take the role of the defects outlined in the previous suggestion. Because the substrate consists of many fibers, the influx of non-solvent would be irregular and the macro-pores might therefore be formed at the solvent/nonsolvent interfacial surface. As a result, unlike the conventional immersion precipitation method, the active layer could not be formed at the solvent/nonsolvent interfacial surface, but instead the patterned surface became the active layer. The displacement of the location of the active layer was confirmed by SEM images of both surfaces of a prism-patterned membrane prepared by the modified method illustrated in Figure III-5. The size of pores at the opposite side of the patterned surface (Figure III-5b), even at lower magnification (X50

magnification), was visually seen to be much larger even at lower magnification (X50 magnification) than that found at the patterned surface (Figure III-5a.)

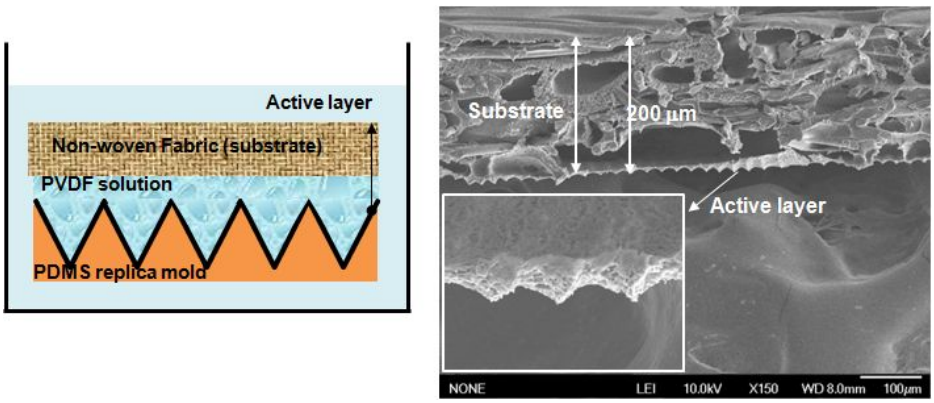

Figure III-4. The location of the active layer in the modified immersion precipitation method and the cross-sectional SEM image of the prism-patterned membrane.

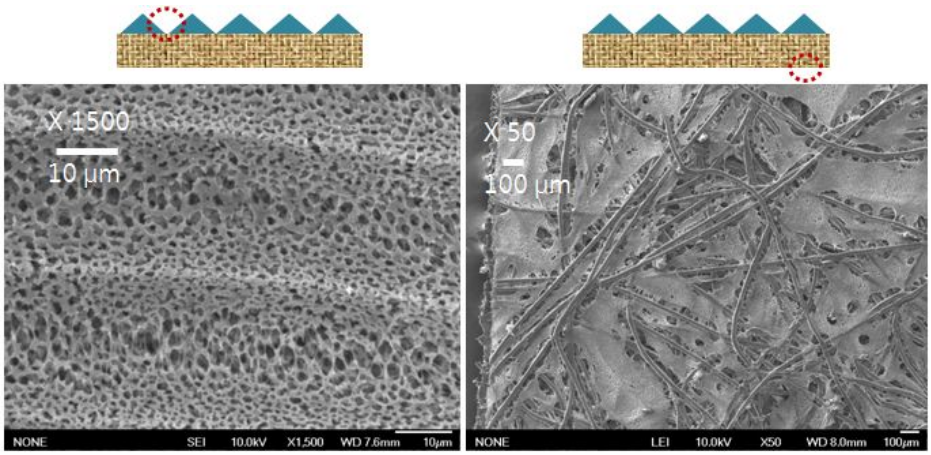

(a) **(b)**

Figure III-5. SEM images of two sides of the prism-patterned membrane prepared by the modified immersion precipitation method: (a) prism-patterned surface, (b) opposite side of the patterned surface.

III.3.2. Variables affecting the fidelity of a patterned membrane

In a patterned membrane, pattern fidelity should be an important parameter in evaluating the surface morphology of the membrane. Pattern fidelity is usually defined by the ratio of the pattern size (width or height) in the replica mold to that (width or height) of the prepared membrane surface. In this study, to determine pattern fidelity we averaged both ratios obtained for width and height, respectively. Particularly in the immersion precipitation method, parameters such as the composition and temperature of nonsolvent, the concentration of a polymer, and additives have been known to be closely related to membrane morphology (i.e., pattern fidelity). In order to optimize pattern fidelity, we focused on polymer concentration in the casting solution because it should be a main factor affecting pattern fidelity in a lithographic method (Vogelaar et al. 2003).

Accordingly, three prism-patterned membranes were prepared using different PVDF concentrations (Table 1) and compared with each other in terms of morphology and pattern fidelity. The pattern fidelities were found to be 0.85, 0.96, and 0.72 with corresponding PVDF concentrations of 10, 15, and 20 wt %, respectively (Figure III-6). The higher PVDF concentration (20 %) gave rise to the mixed morphology of bicontinuous and cellular forms as well as relatively lowers fidelity (Figure III-6c). In contrast, the lower PVDF concentration (10, 15 %) resulted in a typical bicontinuous morphology as well as relatively higher fidelity (Figure III-6a, 6b).

Frank and Keller, based on thermodynamics, suggested that the higher polymer concentration would yield a cellular morphology because the polymer has a tendency to aggregate and grow from random nuclei during the liquid–liquid demixing, whereas intermediate polymer concentrations yield a bicontinuous network structure because spinodal decomposition takes place (Frank and Keller 1988). The concept propounded by Frank and Keller coincides well with the morphologies and fidelities of PVDF patterned membranes as shown in figure III-7. When the PVDF concentration was the highest at 20 %, the polymer could not completely fill the prism-patterned replica (Figure III-7a), which made the cellular morphology of the membrane had a relatively lower fidelity (0.72) (Figure III-6c). In contrast, when the PVDF concentration was at an intermediate level of 10~15 %, the polymer was able completely to fill the prism-patterned replica (Figure III-7b) without the aggregation and growth of the polymer (i.e., spinodal decomposition), which made a membrane of bicontinuous morphology with relatively higher fidelity (0.85~0.96) (Figure III-5a, 5b). However, a substantial mass of PVDF might be necessary to form a smooth and defect-free polymer network in the patterned membrane. The patterned membrane shown in figure III-6a highlights that a minimum concentration of PVDF might be necessary to avoid defects in a patterned membrane of bicontinuous morphology. Therefore, we used the composition of polymer solution 2 (15 %) in the preparation of patterned membranes for the following tests.

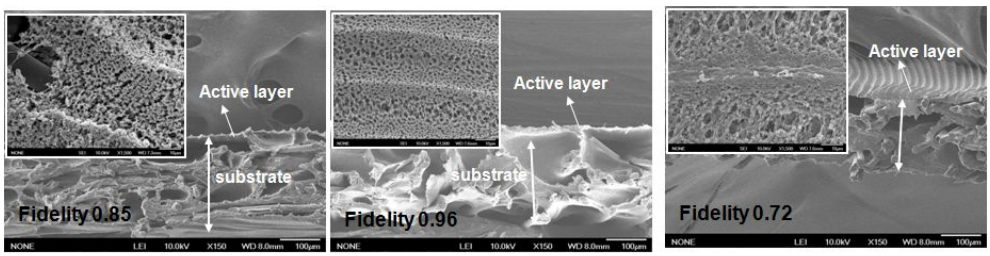

(a) **(b)** **(c)**

Figure III-6. The cross-sectional SEM images of membranes prepared with three kinds of polymeric solutions using the modified immersion precipitation process. (a) Solution 1 (PVDF 1g, DMF 6 g, Acetone 3 g); (b) solution 2 (PVDF 1.5 g, DMF 5.5 g, Acetone 3 g); and (c) solution 3 (PVDF 2 g, DMF 5 g Acetone 3 g).

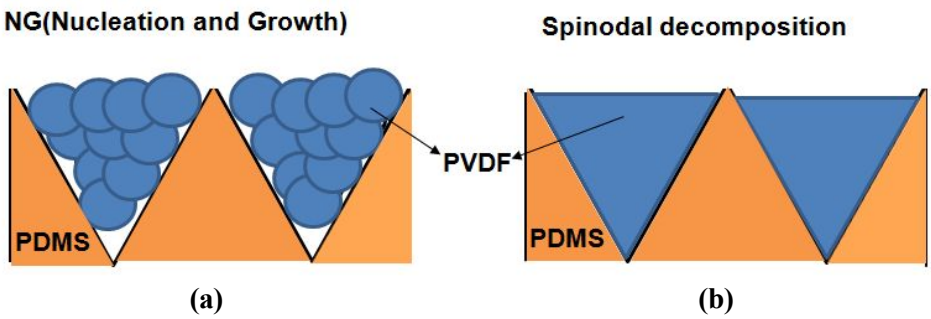

Figure III-7. Difference of patterned membrane morphology according to coagulation mechanism. (a) Nucleation and growth, and (b) spinodal decomposition.

Table 1. Composition of three kinds of polymeric solution used in the preparation of patterned membranes

	PVDF	DMF	Acetone	Concentration of PVDF
Solution 1	1 g	6 g	3 g	10 wt%
Solution 2	1.5 g	5.5 g	3 g	15 wt%
Solution 3	2 g	5 g	3 g	20 wt%

III.3.3. Factors affecting pattern fidelity

III.3.3.1 Molecular weight of a polymer in the casting dope

Three polymeric solutions with different molecular weights of PVDF (S1, S2, and S3) were prepared to investigate the effect of the molecular weight of PVDF on pattern fidelity in the preparation of patterned membranes. Each solution had the same polymer concentration (10 wt%), but the molecular weights of the polymers were 180, 275, and 430 kDa, respectively. Each PVDF solution was cast onto the PDMS replica mold and the nascent membrane was directly dipped into a water bath to induce phase inversion. The morphological changes over the cross-section of the membrane were observed depending on the molecular weight of PVDF. First, the patterned membrane prepared with the lowest molecular weight of 180 kDa showed a finger-like structure (Figure III-8a), whereas those with the higher molecular weights of 275 kDa (Figure III-8b) and 430 kDa (Figure III-8c) had a sponge-like structure. It is well-recognized that the phase inversion rate declines with an increase in polymer molecular weight because the increased viscosity of the polymeric solution restricts the exchange between solvent and non-solvent during the coagulation process. As a slow phase inversion rate impedes the propagation of fingers from the interface between the polymer solution and the non-solvent toward the bottom surface, the morphology in the sub-surface layer changes from finger-like to sponge-like with an increase in polymer molecular weight, as shown in figure III-8. Second, an increase in the molecular weight of

PVDF gave rise to a decrease in Area Fidelity from 0.90 to 0.20 (Figure III-8). An interesting point is that the molecular weight of a polymer affects the phase inversion rate, which in turn influences the pattern fidelity (Bikel et al. 2009, Park et al. 2005).

In order to elucidate in more detail the dependency of pattern fidelity on the molecular weight of a polymer, "Area Fidelity" was further subdivided into "Width Fidelity" and "Height Fidelity" which were defined in section 2.3. By closely examining the shape of the triangle in the prism pattern in Figure III-8, we observed that as the molecular weight of PVDF increased from 180 kDa (S1) to 275 kDa (S2) and to 430 kDa (S3), the width of the triangles in the prism pattern (i.e., "Width Fidelity") did not change substantially (0.90~0.78), but the height of the triangles (i.e., "Height Fidelity") decreased significantly (0.90~0.25), as shown in Table 2. To explain the difference in pattern fidelity shown in Table 2, the correlation between phase inversion rate and pattern fidelity is illustrated in figure III-9.

During the phase inversion process, the demixing (or phase inversion) rate in S3 should be slower than those in S1 or S2 due to its higher viscosity resulting from its higher molecular weight. Consequently, we could imagine that the order of the demixing rate would be S1 > S2 > S3. According to theory of membrane formation by Termonia et al. and Reuvers et al., if the demixing rate is slow, the coagulation of the polymer (PVDF) progresses through nucleation and growth, as shown in Figure III-9b. Because the formation of nuclei or the

coagulation of PVDF is initiated at the non-solvent (water)/polymeric solution interface, which is the opposite side of the patterned surface, the dissolved polymer would continuously diffuse up towards nuclei to make them grow. Consequently, the concentration PVDF near the patterned surface on the PDMS replica mold would become insufficient to form the same pattern as the replica, resulting in a lower "Height Fidelity" (Figure III-8c and Figure III-9b). In contrast, when the demixing rate is faster (S1), the coagulation of the polymer (PVDF) progresses quickly by spinodal decomposition and thus a sufficient amount of PVDF near the PDMS pattern surface would not have enough time to diffuse up to the opposite side, but would rather maintain in the triangle of the prism pattern to form nearly the same pattern as the replica (Figure III-8a and Figure III-9a).

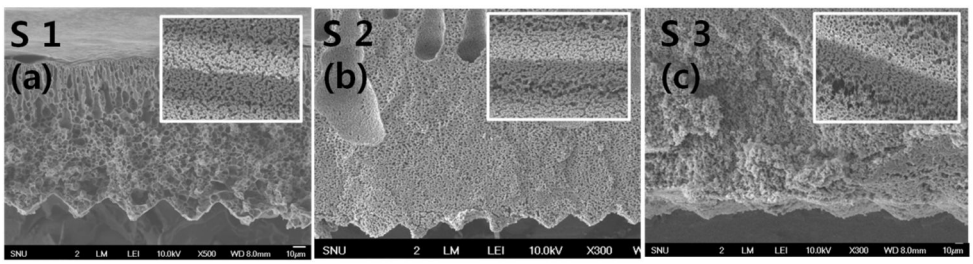

Figure III-8. Morphological changes in the prism-patterned membrane prepared from a 10 wt% polymeric solution consisting of different molecular weight polymers Mw: (a) 180 kDa, (b) 275 kDa, (c) 430 kDa

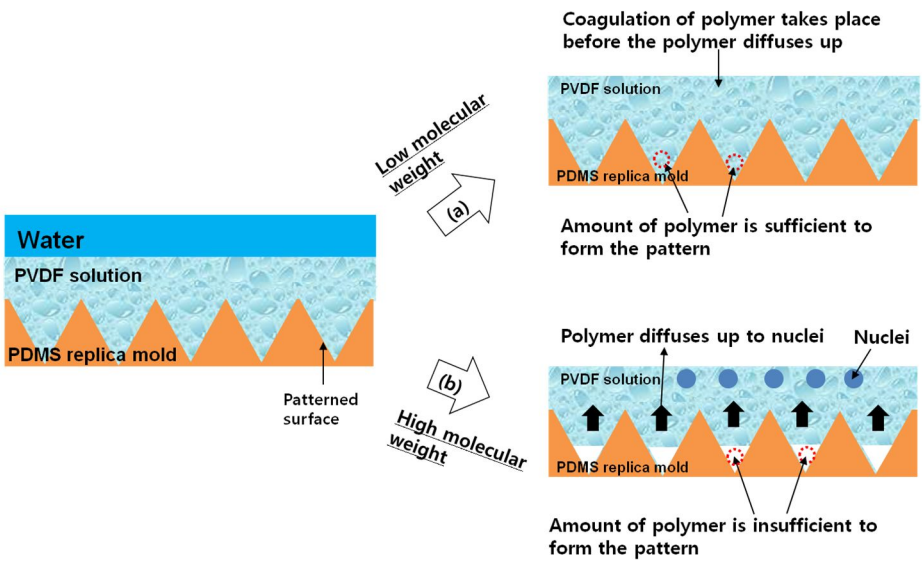

Figure III-9. Mechanisms of pattern formation as a function of the molecular weight of the polymer: (a) low molecular weight (180 kDa), (b) high molecular weight (275 and 430 kDa).

Table 2. Comparison of the width and height in three patterned membranes.

	Width (μm)	Height (μm)	Width Fidelity	Height Fidelity
S 1 (180k Da)	42-45	16-18	0.84-0.90	0.80-0.90
S 2 (275k Da)	39-44	8-12	0.78-0.88	0.50-0.60
S 3 (430k Da)	39-42	4 - 7	0.78-0.84	0.25-0.35

III.3.3.2 Concentration of a polymer in the casting dope

In the previous section, the decrease in "Area Fidelity", especially "Height Fidelity" with a higher molecular weight of the polymer was attributed to an insufficient amount of PVDF in the triangular region in the PDMS replica mold. Hence, it was interesting to determine the pattern fidelity when the concentration of the polymer (PVDF) in the casting dope was increased. Three casting dopes with different molecular weights of 180 kDa (S4), 275 kDa (S5), and 430 kDa (S6) were prepared in a similar way to those in S1~S3, except that the polymer concentrations were maintained at 15 wt% in all casting dopes. Figure III-10 shows the SEM images of three patterned membranes prepared with S4, S5, and S6. Similar to membranes prepared with S1, S2 and S3 in Fig. 4, the membrane structure shifted from finger-like (Figure III-10a) to sponge-like (Figure III-10c) as the molecular weight increased. Because of this structural change, we could imagine a difference in the mixing rate during the phase inversion process. However, the "Area Fidelity" was maintained at a high value (>0.91) regardless of the molecular weight of the polymer. Although the diffusion of the polymer from the patterned surface to the opposite side could take place at a higher molecular weight of the polymer (S6), the amount of residual polymer at the patterned surface would be sufficient to maintain the original pattern of the replica mold, taking into account the higher polymer concentration of 15% compared with that of S1-S3 (10%). It was concluded that the pattern fidelity is in close association with both the concentration and the molecular weight of the polymer in the casting dope (Wang

et al. 2009, Song et al. 2007).

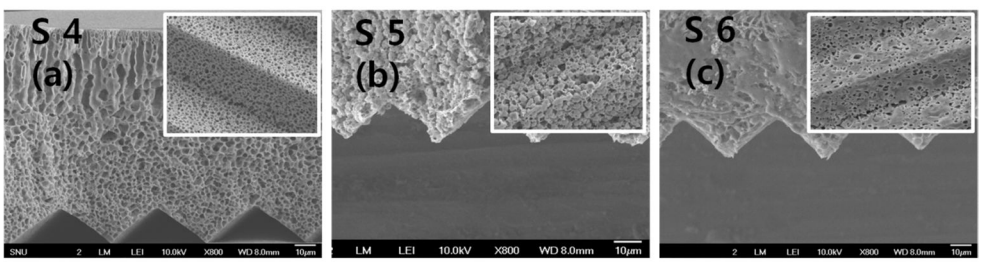

Figure III-10. Morphological changes in the prism-patterned membrane prepared from a 15 wt% polymeric solution consisting of different molecular weight polymers Mw: (a) 180 kDa, (b) 275 kDa, (c) 430 kDa

III.3.3.3 Hydrophilicity between the polymeric solution and replica mold

In the preparation of the patterned membrane, the spreadability of a polymeric solution on the PDMS replica mold, i.e., extent of contact between a cast dope and a solid substrate was presumed to be one of key factors affecting the pattern fidelity. It was because the pattern became easily distorted when the polymeric solution did not spread out uniformly on the substrate. Thus, we suspected that the interaction between the polymeric solution and replica mold might affect the formation of uniform polymer film, which in turn affect the pattern fidelity substantially. To verify the above hypothesis, PVDF solution was cast onto four solid substrates with different hydrophilicity. They were PDMS (Poly(dimethylsiloxane)), PUA (poly(urethaneacrylate)), PS (polystyrene), and PDMS replica mold with a hydrophilized surface. The contact angles were measured for four solid materials without pattern (Figure III-11). The PUA mold shows the lowest contact angle, i.e., the highest hydrophilicity, whereas the PDMS shows the lowest hydrophilicity among them. The prism pattern was introduced into all four molds to make patterned membranes. Figure III-12 shows the SEM images of the resulting four prism patterned membranes. The membrane fabricated with the most hydrophilic mold (PUA) yielded the lowest pattern fidelity among four membranes (Figure III-12d). In this membrane, even a little trace of prism pattern could hardly been observed. In contrast, the membrane fabricated with the hydrophobic mold (PDMS) yielded the highest pattern fidelity of all four

membranes (Figure III-12a). The membranes fabricated with the intermediate hydrophobic molds (PDMS with hydrophilized surface and PS) showed prism patterns with some defects (Figure III-12b & 12c). The results seem to be closely related to wetting phenomenon, indicating the degree of affinity between a casting dope and a mold surface. Since the PVDF polymer in the polymeric solution is a hydrophobic material, the PVDF can be spread out more uniformly on the more hydrophobic surface (Li et al. 2008, Lang et al. 2013). In contrast, the PVDF on the hydrophilic surface would be aggregated rather than be spread out uniformly. Consequently, the patterns prepared on the hydrophilic replica molds showed twisted or distorted shapes (Figure III-12b & 12c)

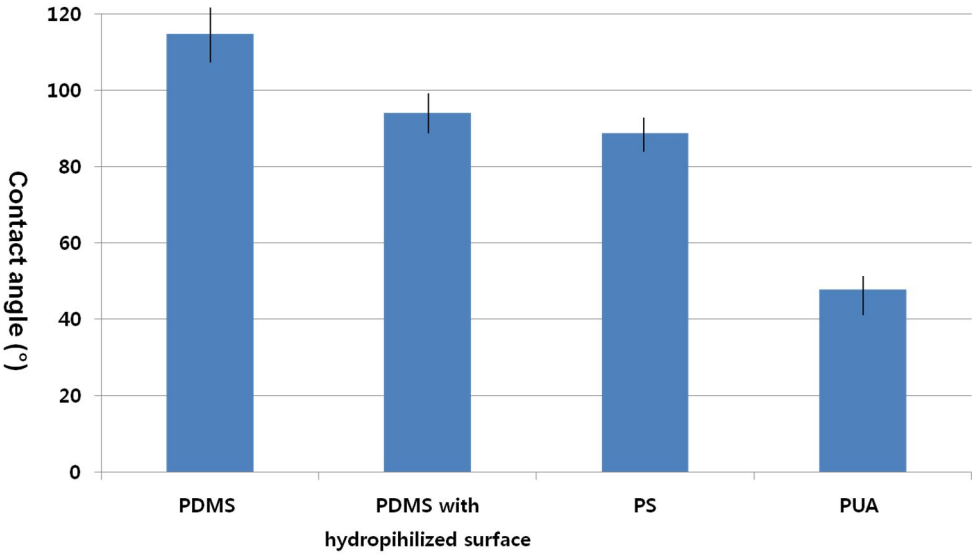

Figure III-11. Comparison of the contact angle between different replica materials (n=5)

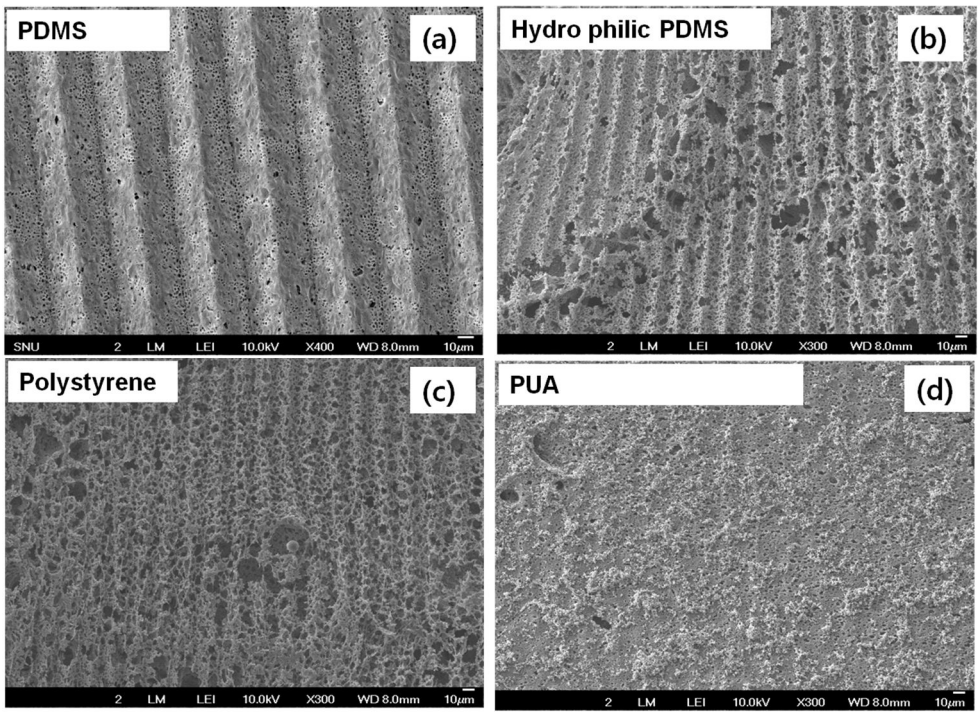

Figure III-12. SEM images of prism-patterned membranes prepared from four different replica molds: (a) the original PDMS replica mold, (b) the hydrophilic PDMS replica mold, (c) the polystyrene replica mold, (d) the PUA replica mold

III.4. Conclusions

The purpose of this chapter was to prepare the patterned membrane and optimize the fidelity of pattern.

- A novel micro-patterned membrane with a pyramid or prism pattern was prepared using a soft-lithographic and immersion precipitation method. Because a soft-lithographic technique was applied in preparation of the membrane, a diverse and small (10–20 μm) pattern could be introduced onto the membrane surface. In preparation of the patterned membrane, a new modified phase inversion process was developed because the conventional phase inversion process is limited by the reversed location of the active layer.

- The molecular weight of the polymer in the dope solution is affected by the phase inversion rate, which in turn influences pattern fidelity. In other words, the lower the molecular weight of a polymer, the faster the phase inversion rate, yielding greater pattern fidelity.

- When the hydrophilicity of the polymeric solution and the patterned replica mold is similar, the patterned membrane has greater pattern fidelity.

Chapter IV

Characterization of patterned membrane and application to membrane process

IV.1. Introduction

In the previous chapter, we have prepared diverse patterned membrane using by modified phase inversion methods. Even though the patterned membrane was prepared successfully, characteristics and performance of patterned membrane should be investigated. In this chapter, various characteristics of patterned membrane were investigated to elucidate its antifouling potential. Pore-size distribution and membrane thickness will be tested. Also, the performance of patterned membrane such as pure water flux will be investigated.

IV.2. Experimental Section

IV.2.1. Membrane characterization

The morphology of the membrane was observed by a Scanning Electron Microscope (SEM) (JSM-6701F, Jeol, USA). To obtain a cross sectional image, the membrane was frozen using liquid nitrogen, and was then coated with gold–platinum by a sputtering machine. The pore size distribution of a patterned membrane was measured by a capillary flow porometer (CFP-1500AEL, PMI, USA). The membrane sample was wetted using Galwick® solution of which the surface tension was adjusted to 15.9 dyne/cm. The wetted sample was placed in a sealed chamber and nitrogen gas was permeated until the bubble point was detected. The pore-size distribution of the membrane was measured using the 'dry up' and 'wet up' modes, and the pore diameter was calculated using equation (3):

$$D = \frac{4\gamma\cos\phi}{P} \qquad \text{----------} \qquad (3)$$

where D is the pore diameter, γ the surface tension of the wetting solution, ϕ the contact angle of the wetting solution, and P the differential gas pressure.

IV.2.2. Membrane performance

The patterned and flat membranes were tested in a cross-flow microfiltration (MF) system, as depicted in Figure IV -1. The test cell was 64 mm in length, 22 mm in width and 2 mm in depth. The effective surface area of the test membrane was 14.1 cm^2. At the various transmembrane pressures (TMP) (10, 15, 20, 25 kPa), the water fluxes of flat and patterned membranes were measured in a cross-flow MF system and compared with each other for each TMP. The mixed liquor of activated sludge was also removed from the laboratory. Scale MBR (Figure IV -1b) was fed to the cross-flow MF system under the total recycle mode (Figure IV -1a). The retentate was recirculated at a cross-flow rate of 0.05 m/s (Reynolds number = approx. 1000). After running the cross-flow MF for either 2 or 4 h, the tested membranes were taken out of the modules and stained ready for confocal laser scanning microscopy (CLSM) observation (Kim et al. 2011).

The laboratory-scale MBR was also run under continuous mode at a constant flux of 12 L / ($m^2 \cdot$ hr) to evaluate the performance of patterned and flat membranes (Figure IV -1b). The two identical membrane modules, with flat and patterned membranes respectively, were submerged vertically in the aerobic tank. Other specific operating parameters for the continuous MBR are summarized in Table 3 (Hwang et al. 2008).

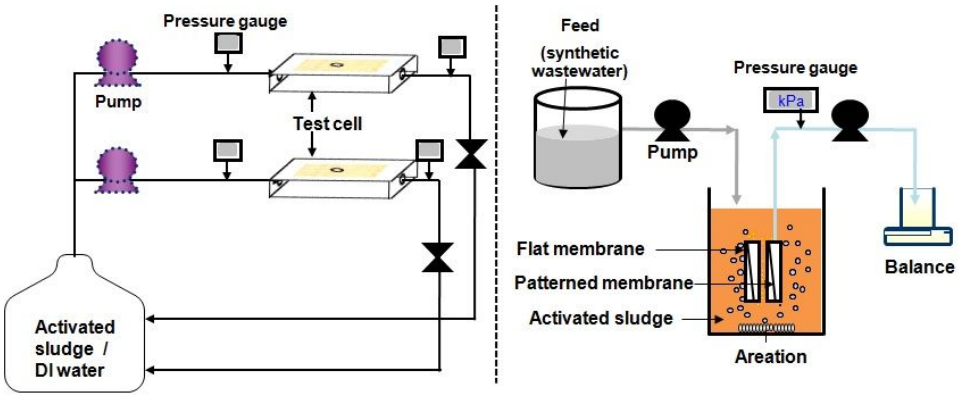

Figure IV-1. Schematic diagrams of laboratory-scale of (a) a cross microfiltration system, and (b) a submerged MBR.

Table 3. Operating conditions of the continuous MBR.

Concentration of the mixed liquor-suspended solids (MLSS)	6500 (±100) mg / L
Hydraulic retention time (HRT)	8 hr
Solid retention time (SRT)	30 days
Temperature of reactor	20–28 °C
pH	7.0–7.5
Working volume	1.5 L
COD removal efficiency	98 %
Flux	12 L /m^2/h

IV.3. Results and Discussion

IV.3.1. Pore-size distribution and pure water flux of patterned membranes

The pore size distribution, thickness and water flux of patterned and flat membranes were evaluated and compared with each other. All three membranes, including two kinds of patterned membranes (pyramid, prism) and a flat membrane were prepared using the modified method. The cross-sectional SEM images of three membranes revealed clearly that they had almost the same membrane thickness, at about 200 μm, but different surface morphologies: pyramid (Figure IV-2a), prism (Figure IV-2b) and flat (Figure IV-2c). However, the height of apex differed from each other depending on the type of pattern.

The mean pore sizes of the pyramid- and prism-patterned membranes were 0.89 μm and 0.91 μm, respectively (Table 4). Comparing them with that of the flat membrane (0.85 μm), the patterning on the membrane surface did not substantially affect the pore size. However, all the patterned membranes (pyramid, parallel and perpendicular prism) exhibited substantially higher water flux than that of the flat membrane (Figure IV-3). The patterning increased the average water flux by about 20 % in comparison to the flat membrane, regardless of the pattern type. The increase of the membrane surface caused by patterning is directly related to the roughness factor, which is defined as the ratio of the actual and projected

area of a membrane surface. The roughness factors of pyramid- and prism-patterned membranes were calculated to be 1.22 and 1.23, respectively. Thus, the surface area enlarged by patterning leads to a proportional increase in the water flux.

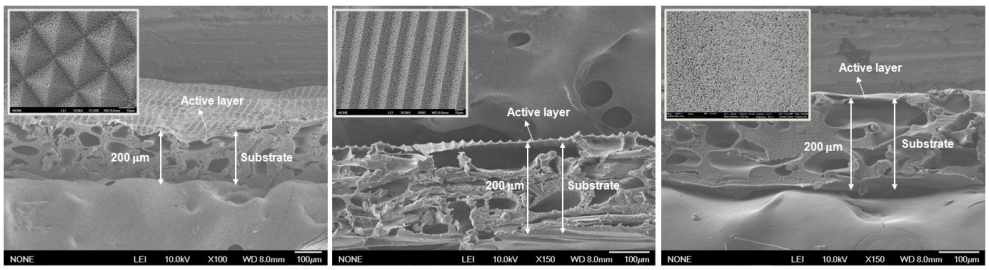

Figure IV-2. Cross-sectional SEM images of two kinds of patterned membrane and flat sheet membrarne. (a) pyramid type, (b) Prism type, (c) flat sheet type. All membranes were prepared by modified immersion precipitation process with the same polymer solution (solution 3; PVDF 1.5g DMF 4.5g Acetone 4g).

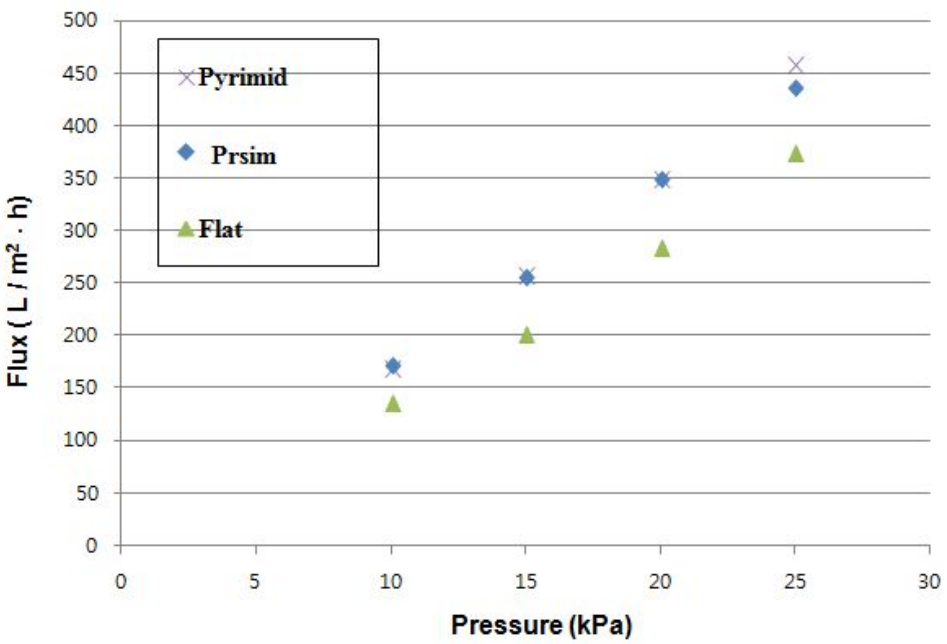

Figure IV-3. Water fluxes of the single flat sheet and the patterned membranes.

Table 4. Composition of three kinds of polymeric solutions used in the preparation of patterned membranes

	Pyramid-patterned membrane	Prism-patterned membrane	Flat membrane
Height of Apex	8.2 - 9.6 μm	9.3 – 9.9 μm	-
Mean pore size	0.89 ± 0.15 μm	0.91 ± 0.22 μm	0.85 ± 0.14 μm

IV.3.2. Mitigation of biofouling with patterned membranes

A cross-flow MF of activated sludge was carried out to compare the extent of biofouling between vertical prism-patterned and flat membranes. The mixed liquor taken from MBR for wastewater treatment was fed to the cross-flow microfiltration in a batch mode with total recycle (Figure IV-1a). Figure IV-4 shows the CLSM images of the used membranes after 2 and 4 hr. The red color represents the membrane surface and the green color represents the microbial cells deposited on the membrane surface. After operation for 2 hr, the flat membrane was substantially covered by the microbial cells, but microbial cells were only deposited in the valley of the vertical prism-patterned membrane. Over the course of operation for 4 h, the flat membrane was almost completely covered with microbial cells, whereas the apex of the prism-patterned membrane mostly remained red, indicating that the patterned surface substantially mitigated the biofouling. The apex of the prism-patterned membrane could therefore act to resist fluid flow and promote local shear, which in turn mitigates the deposition of microbial cells on the patterned membrane surface (Efimenko et al. 2009).

To further investigate the effect of a patterned surface on membrane biofouling, a submerged MBR was run for the flat and pyramid-patterned membranes, monitoring the variations in TMP for both membranes (Figure IV-5). The rise up of the TMP, indicating the extent of membrane biofouling, was significantly delayed in the pyramid-patterned membrane in comparison with that for the flat membrane. After operating of the MBR for 60 hr, the TMP reached 20

kPa in the flat membrane, whereas the TMP remained at the initial value of 5 kPa. The delay in the TMP rise up in the pyramid-patterned membrane was also attributed to local turbulence generated by the patterned surface, which could inhibit the deposition of microbial cells.

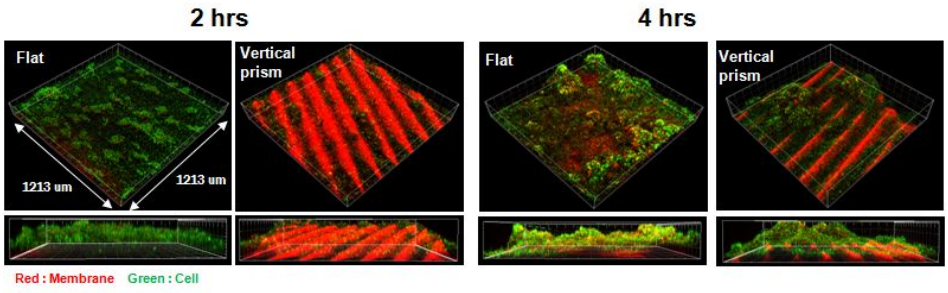

Figure IV-4. CLSM images of the used flat sheet and prism-patterned membranes after 2 and 4 h operations in the cross-flow MF of the mixed liquors taken from MBR.

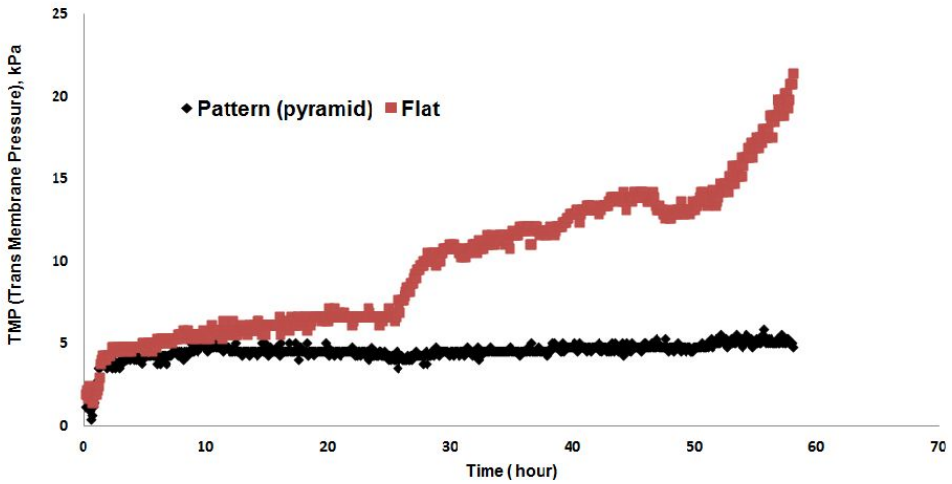

Figure IV-5. TMP profiles of the flat and pyramid-patterned membranes in the continuous submerged MBR for wastewater treatment.

IV.3.3. Relationship between the pattern height and the membrane performance

In previous session, we described how and why the molecular weight and concentration of a polymer in a casting dope can affect the pattern fidelity, particularly Height Fidelity. From a practical point of view, however, it may be interesting to investigate the relationship between the pattern size (i.e., the height of the prism pattern) and membrane performance. For this purpose, we prepared three prism-patterned membranes which were different only in the height of the pattern. First, we prepared three types of PDMS replica molds with different pattern heights using spin coating. The SEM images of three PDMS molds are shown in figure IV-6a, figure IV-6b, and figure IV-6c. The two replica molds in figure IV-6b and figure IV-6c were prepared based on the mold in figure IV-6a as following: the PDMS solution was cast on the prism-patterned PDMS replica mold (figure IV-6a). Then the PDMS solution and PDMS replica mold were spin-coated to fabricate two other PDMS molds with shorter pattern heights under the specific conditions listed in Table 5. Each spin-coated PDMS mold was baked in the oven at 60°C for 2 h. As a result, we obtained two other PDMS molds (Figure IV-6b and Figure IV-6c) in which the pattern heights were decreased by around 25-35% and 75-85%, respectively, whereas their pattern widths did not change substantially compared to those in the original mold (Figure IV-6a). Based on these three replica molds (Figure IV-6a, b, and c), three prism-patterned PVDF membranes were prepared using the polymeric solution S1 (DMF/PVDF, concentration: 10 wt%,

Mw: 180 kDa) at a temperature of 24-25°C and a moisture content of 45-47%. The SEM images of the three prism-patterned membranes which were prepared using each corresponding PDMS mold (Figure IV-6a, b, and c) are shown in figure IV-6a′, b′, and c′, respectively. The heights of the three patterned membranes were 18-20 μm (Figure IV-6a′), 13-15 μm (Figure IV-6b′), and 4-7 μm (Figure IV-6c′), respectively. However, all three patterned membranes maintained relatively high Area Fidelity greater than 0.93 because the molecular weight of PVDF in the casting dope was 180 kDa, which is low enough to form a patterned membrane of high fidelity.

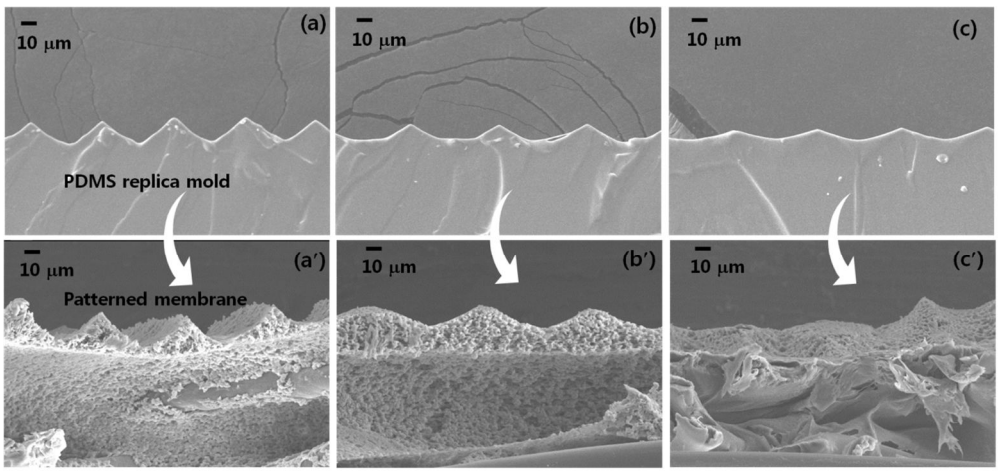

Figure IV-6. SEM images of cross-sections of the replica molds (a, b, c) and the prism-patterned membranes (a′, b′, c′). The height of the prism pattern: a′; 18-20 μm, b′; 13-15 μm, c′; 4-7 μm

Table 5. Specific conditions for spin-coating to fabricate diverse PDMS replica molds with different pattern sizes

Replica Mold	Size of pattern (μm)	Spin coating time (min)	Spin coating rate (rpm)
Fig. 10-a	Width : 50 Height : 20	-	-
Fig. 10-b	Width : 45-50 Height : 10-12	2	5000
Fig. 10-c	Width : 42-48 Height : 3-6	5	5000

IV.3.4. Water flux vs. pattern height

Water fluxes through a non-patterned flat membrane and three prism-patterned membranes with different pattern heights were measured at a TMP of 20 kPa in a cross-flow microfiltration system and compared to one another. As shown in figure IV-7, the water fluxes of the patterned membranes were all enhanced compared with that of the non-patterned membrane. The patterned membrane with the highest pattern height (18-20 μm) showed the highest flux and the patterned membrane with the lowest height of pattern (4-7 μm) showed a similar water flux to that of the non-patterned membrane. The enhancement in water flux of the prism-patterned membranes along with their pattern heights could be attributed to the increase in the membrane surface area due to the increase in the pattern height. This has been also been reported by Cufez et al., who prepared and tested a patterned hollow fiber membrane (Culfaz et al. 2011a, Culfaz et al. 2011b, Culfaz et al. 2010, Culfaz et al. 2011c).

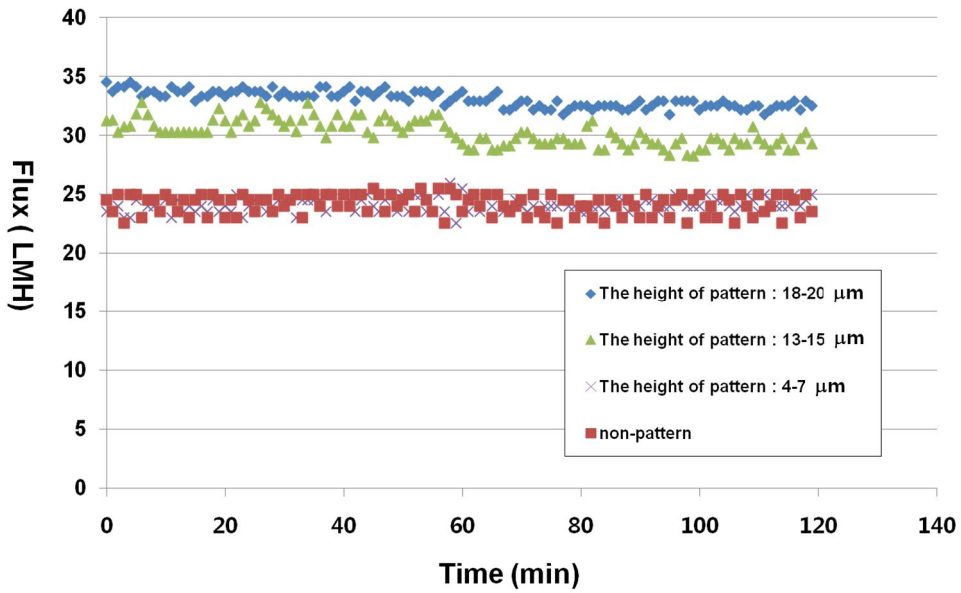

Figure IV-7. Comparison of water flux between three prism-patterned membranes with different pattern heights: (♦) 18-20 μm, (▲) 13-15 μm, (×) **4-7 μm**

IV.3.5. Biofouling vs. pattern height

In order to investigate the effect of pattern height on membrane biofouling, the anti-biofouling characteristic of each patterned membrane was examined with a CDC (cocurrent downflow contactor) filled with *Pseudomonas aeruginosa* PAO1 tagged with green fluorescent protein (GFP) (Kim et al. 2011). Figure IV-8 shows the CLSM images of microbial attachment on the surface of each prism-patterned membrane. On the surface of patterned membrane with the greatest pattern height (18-20 μm), microbial attachment was the lowest (Figure IV-8a), whereas microbial attachment was the greatest on the patterned membrane surface with the shortest pattern height (3-5 μm), as shown in figure IV-8c. This tendency may be related to the degree of shear stress generated by the pattern. Lee et al. reported that local wall shear stress is greater in the upper region of a prism-patterned membrane using numerical simulations. Thus, we numerically simulated the strength of shear stress along the height of the prism pattern.

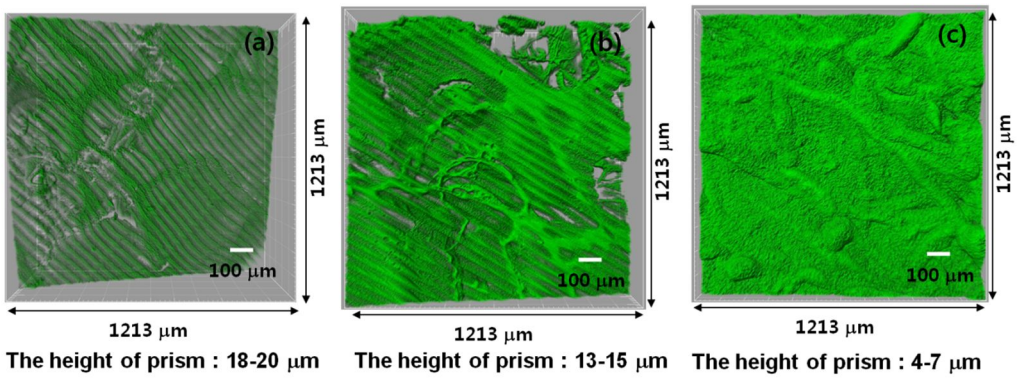

Figure IV-8. CLSM images of prism-patterned membranes with different pattern heights. The height of the prism pattern: (a) 18-20 μm, (b) 13-15 μm, (c) 4-7 μm

IV.4. Conclusions

The purpose of this chapter was to characterize the patterned membrane and test the performance of patterned membrane. Based on the results of this study, the following conclusions were made:

- Pure water flux of patterned membrane was significantly increased because the effective membrane area increased by patterning.

- The mean pore sizes of the pyramid- and prism-patterned membranes were almost same as that of non-patterned membrane. It indicated that the patterning on the membrane surface did not substantially affect the pore size

- In cross-flow filtration, the flat membrane was almost completely covered with microbial cells, whereas the apex of the prism-patterned membrane mostly remained uncovered. It indicates that the patterned surface could substantially mitigate the biofouling.

- In lab-scale MBRs, The delay in the TMP rise up in the pyramid-patterned membrane was also attributed to local turbulence generated by the patterned surface, which could inhibit the deposition of microbial cells.

- On the surface of patterned membrane with the greatest pattern height, microbial attachment was the lowest, whereas microbial attachment was the greatest on the patterned membrane surface with the shortest pattern height

Chapter V

Applying diverse prism pattern to membrane process to understanding antifouling mechanism of patterned membrane

V.1. Introduction

In the previous chapter, various characteristics of patterned membrane were evaluated and performance of patterned membrane in lab-scale membrane process was tested. In addition, the relationships between pattern height and membrane performance were investigated.

In this chapter, the diverse prism pattern which has different pattern size will be applied to cross-flow system. We have investigated deposition of latex particle in response to change of Reynolds number or particle diameter. Comparing the mass of attached particle in diverse prism pattern with non-patterned case, we want to find the parameters affecting antifouling ability of patterned membrane.

V.2. Experimental Section

V.2.1. Cross-flow filtration system

The patterned and non-patterned membranes were tested in a cross-flow microfiltration (MF) system, as depicted in figure V-1. The test cell was 64 mm in length, 22 mm in width and 2 mm in depth. The effective surface area of the test membrane was 14.1 cm^2. The fouling test was performed during 2 hr and the surface of observed by optical microscope or CLSM. After the operation, the attached latex particles was released from the membrane surface and collected in DI water bath. The turbidity of these samples was measured and it is converted into mass of deposited particle. At this time, the calibration curved between mass of deposited particle and turbidity was illustrated in figure V-2.

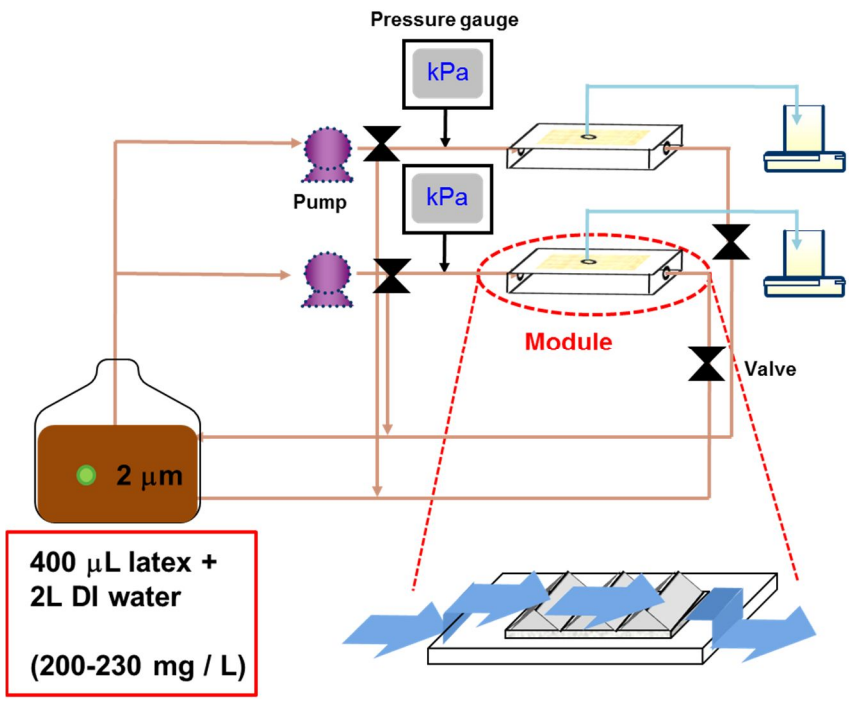

Figure V-1. The schematic diagram of lab-scale cross flow MBRs

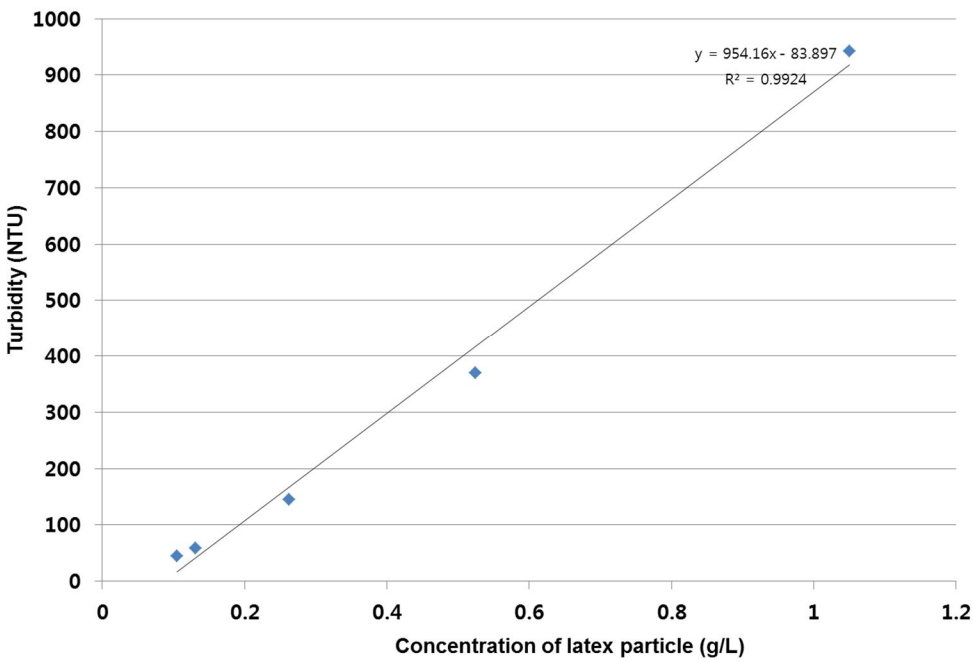

Figure V-2. The calibration curved between mass of deposited particle and turbidity

V.2.2. Type of pattern

In this experiment, four kinds of prism pattern were used (Figure V-3).

(a) The prism pattern of 25 μm width and height without interval.

(b) The prism pattern of 400 μm width and height without interval.

(c) The prism pattern of 400 μm width and height with 400 μm interval region between the prism patterns. (prism pattern width : interval region = 1:1)

(d) The prism pattern of 400 μm width and height with 800 μm interval region between the prism patterns. (prism pattern width : interval region = 1:2)

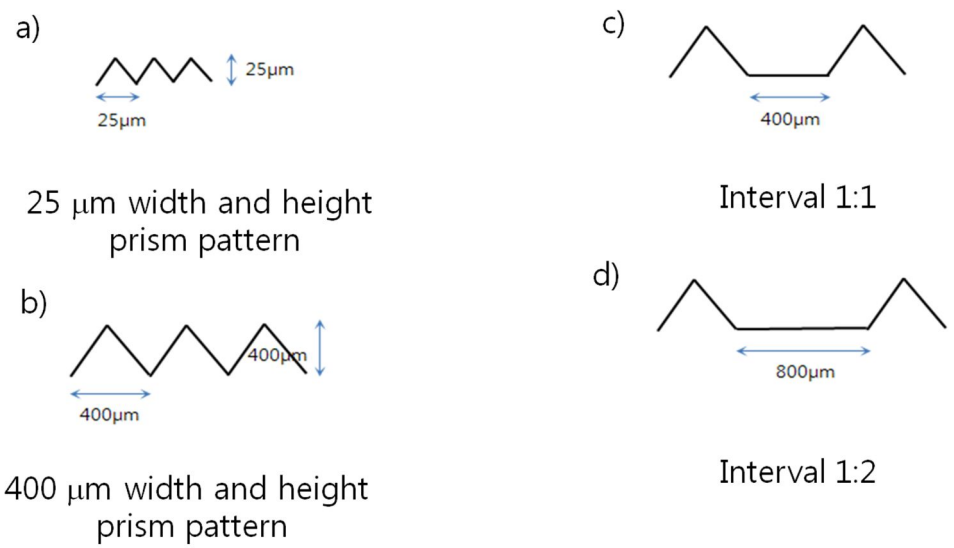

Figure V-3. Schematic diagrams of diverse prism pattern. Width and height of the prism pattern was a) 25 μm, b) 400 μm. c) and d) contains the interval region between the prism patterns. The width of interval is c) 400 μm, d) 800 μm

V.3. Results and Discussion

V.3.1. Pattern size vs. membrane fouling

Firstly, the effect of size in patterned membrane (pattern height and width) on membrane fouling was investigated. Two kinds of prism pattern were chosen; one with 400 μm width and height of prism and the other with 25 μm width and height of prism. The non-patterned membrane was used as control group. Each membrane was fixed in cross-flow module and the feed containing latex particle with 2 μm diameter was circulated by the pump. After the 2 hrs operation, the deposited latex particles on each membrane were collected and their masses were measured. Figure V-4 represents the total mass of deposited particles when the filtration was operated under Re = 600. As a result, both patterned membranes showed higher antifouling ability than non-patterned membrane case. Especially, the amount of total attached particle mass was lowest in the 25 μm width and height prism pattern case. The reason why the 25 μm pattern shows higher antifouling ability than that of 400 μm pattern case was concerned with area of valley region in prism pattern. At previous session, we confirmed that the foulant was easily deposited at valley region. Thus we could predict that the area of valley region was related with the total mass of deposited latex particle. The area of valley region in 400 μm prism pattern was about 8×10^4 μm^2 and that of 25 μm prism pattern was about 313 μm^2. Taking account into the ratio of valley region area was

255, it is reasonable that the amount of attached foulant in 400 μm prism pattern was higher than that of 25 μm prism pattern case.

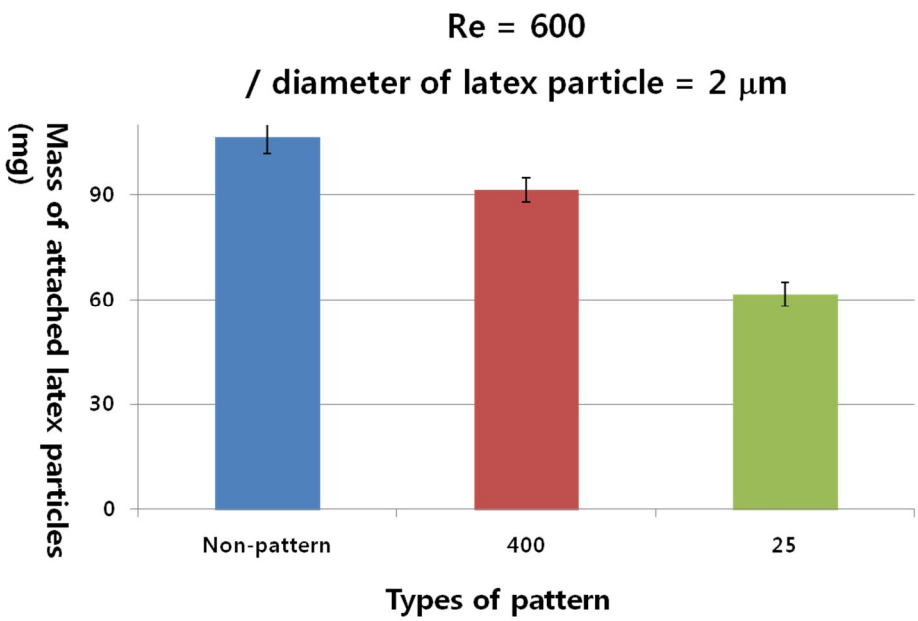

Figure V-4. Comparison of mass of deposited latex particle. The Reynolds number of system was 600 and the feed containing 2 μm latex particles.

V.3.2.Pattern size, Reynolds number vs. membrane fouling

The same cross flow experiment was repeated under Re = 1600. Figure V-5 shows the result of total mass of deposited particles at Re = 1600. With increasing the Reynolds number from 600 to 1600, the linear velocity of cross-flow increases from 0.1 - 0.3 m/s to 0.4 - 0.5 m/s. It is well known that the Reynolds number of cross flow has considerable influence on the short term attachment of particle. According to previous studies, the attachment of particle decreased with increasing Reynolds number. In our experiment, also, the same behavior of membrane fouling can be seen comparing the total attached particle mass in figure V-4 with figure V-5. However, depending on the applied pattern size, the decreased amount of particle was different with each other. In the case of non-pattern and 25 μm prism pattern, the mass of total attached particle was decreased by 40% (figure V-4 and figure V-5). In 400 μm width and height prism pattern, the mass of total attached particle was dramatically decreased by 60 %. This different performance of 400 μm and 25 μm prism pattern was closely associated with pattern size. Lee et al reported that the shear stress and velocity profile could be changed by the pattern size. They confirmed that the higher pattern height could generate higher shear stress. Based on the results reported by Lee et al, we could apply their hypothesis to our results. In the case of 400 μm pattern, the pattern was a larger obstacle to the feed flow than 25 μm pattern. Thus, it could generate higher shear stress against the high velocity of feed flow. The shear stress generated by the pattern finally

disturbed the deposition of particles

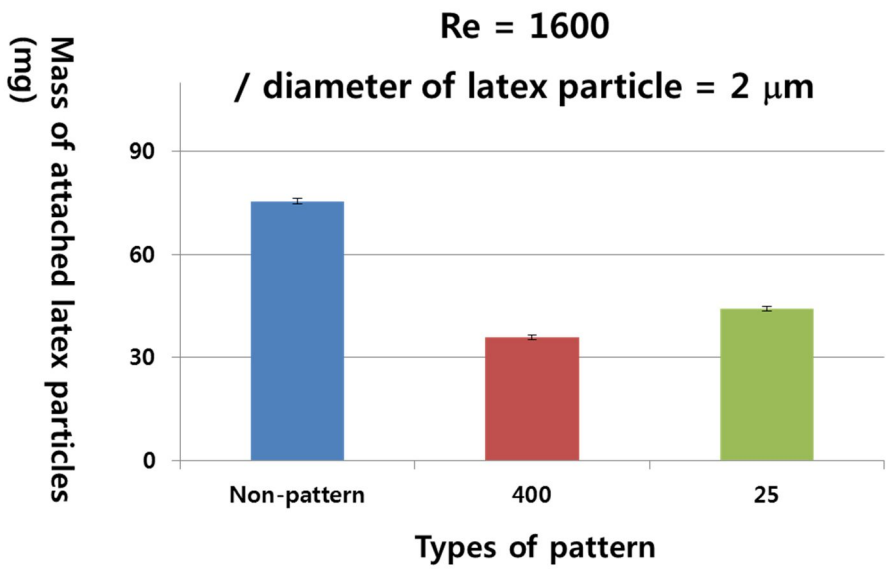

Figure V-5. Comparison of mass of deposited latex particle. The Reynolds number of system was 1600 and the feed containing 2 μm latex particles.

V.3.3.Pattern size, Reynolds number, particle size vs. membrane fouling

Considering the results of previous session, it is possible to conclude that the antifouling effect of prism pattern was optimized when the size of pattern and Reynolds number of system was high. However, in real wastewater, the foulant has size distribution. Thus it is necessary to evaluate the different size of latex particle with respect to the patterned membranes. The same experiment was repeated using 10 μm latex particles. Figure V-6 shows the result of particle deposition with 10 diameter latex particles. At this time, the Reynolds number of system was 600 and 1600. As shown in figure V-6b and 6d, the mass of deposited latex particle on the patterned membrane surface was lower than that of non-patterned membrane. Thus we could conclude that the antifouling effect of patterned membrane was still persisted in this test. Another remarkable point in figure V-6b and 6d is that the antifouling ability of 25 μm prism pattern was significantly increased, unlike previous 2 μm latex particles test. Independent of Reynolds number, the latex particles could scarcely deposit on the 25 μm prism pattern. This remarkable antifouling ability of 25 μm prism pattern might be closely associated with valley region of prism pattern. As shown in figure V-6b and 6d, it is hard for many latex particles to deposit in valley region of 25 μm prism pattern because the area of valley region is limited. Only two or three particles could deposit in valley region and, if it is deposited, it is easily removed by the collision with other latex particles.

Thus, if there are large foulant dominantly, the small pattern size could have high antifouling ability.

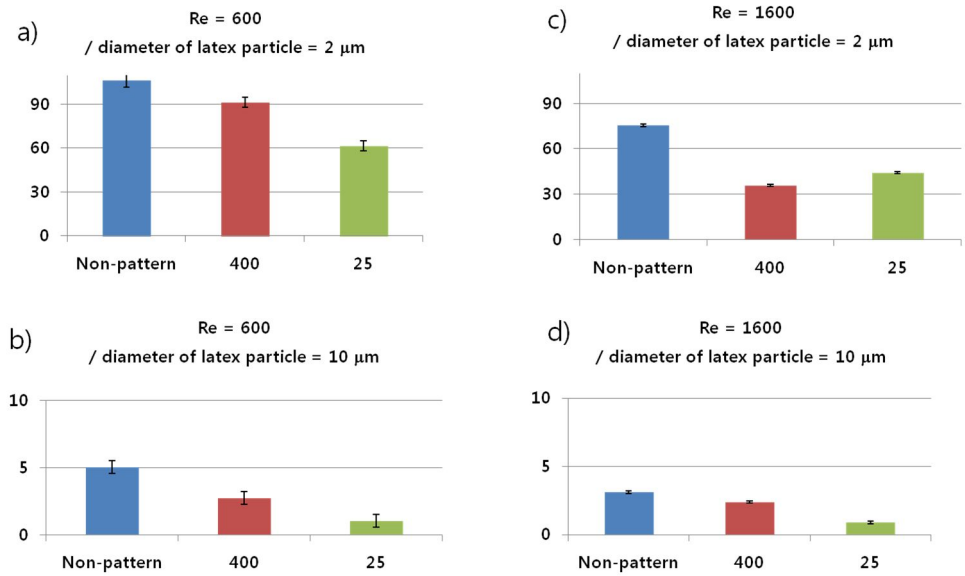

Figure V-6. Comparison of mass of deposited latex particle. The operating conditions were a) Re = 600, diameter of latex particle = 2 μm, b) Re = 600, diameter of latex particle = 10 μm, c) Re = 1600, diameter of latex particle = 2 μm, d) Re = 1600, diameter of latex particle = 10 μm

V.3.4. Interval region between patterns vs. membrane fouling

In this session, we have investigated that the behavior of latex particle in response to change of shape of valley region. In this experiment, three kinds of prism pattern which are b, c, and d shown in Figure V-3 were chosen. Other crossflow condition was maintained same as previous experiment.

Firstly, the effect of interval on deposition of latex particle was evaluated. As shown in Figure V-7, when the Reynolds number was 600, significant particle deposition was observed in two kinds of interval prism pattern. Surprisingly, the prism pattern with interval showed even higher particle deposition than non-patterned membrane. In fact, this result was reasonable considering the area of valley region in interval prism pattern. Because the area of valley region of 1:2 interval prism pattern was 5 times higher than that of no-interval prism pattern, the latex particle easily deposited on the interval prism pattern. Therefore, under low Reynolds number, introducing the interval between prism patterns was impractical.

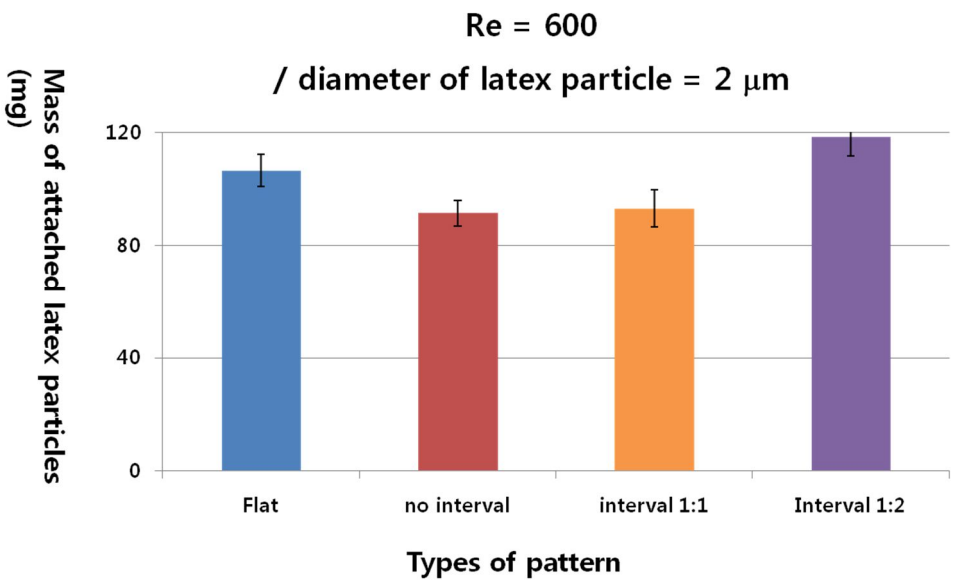

Figure V-7. Comparison of mass of deposited latex particle. The operating conditions were Re = 600, diameter of latex particle = 2 μm

V.3.5.Interval region, Reynolds number vs. membrane fouling

Increasing the Reynolds number from 600 to 1600, the same experiment was repeated. Figure V-8 shows the results of latex particle deposition under two Reynolds numbers (600 and 1600). In the case of non-patterned membrane, mass of deposited latex particles was decreased by 30% with increasing the Reynolds number. We could regard that this decrease is caused by increasing Reynolds number. However, the deposition of latex particle in interval prism pattern was dramatically decreased by 80%. Considering greater decrease in mass of attached particles in interval pattern than non-pattern, it is suggested that there is additional parameters affecting antifouling ability of patterned membrane. In order to elucidate this phenomenon, additional analysis should be carried out. According to previous study of Lee et al., the antifouling ability of patterned membrane was closely related with the shear stress and vortex generated by the pattern on the membrane surface. Thus we could assume that the additional shear and vortex was generated in interval prism pattern. As a future work, it is necessary to analyze the additional shear stress and vortex formation using modeling tools.

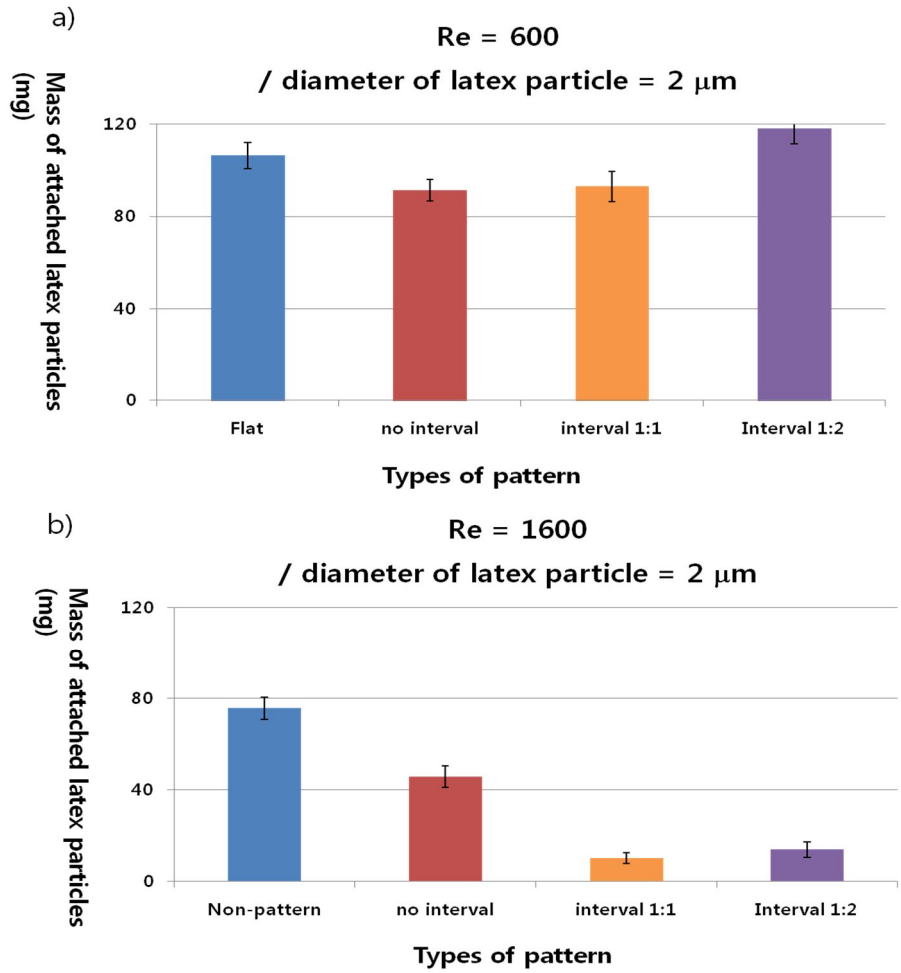

Figure V-8. Comparison of mass of deposited latex particle. The operating conditions were a) Re = 600, diameter of latex particle = 2 μm, b) Re = 600, diameter of latex particle = 10 μm

V.4.Conclusions

The purpose of this chapter was to apply the diverse prism pattern to the cross-flow filtration for understanding the antifouling mechanism of patterned membrane. Based on the results of this study, the following conclusions were made:

- 25 μm width and height prism pattern and 400 μm width and height prism pattern, both patterned membranes show higher antifouling ability that non-patterned membrane case. However, small prism pattern has higher antifouling ability because small prism pattern has small valley region.

- With increasing the Reynolds number from 600 to 1600, the mass of deposited latex particle was decreased. However, depending on the applied pattern size, the decreased amount of particle was different with each other.

- Using 10 μm latex particles, the mass of deposited latex particle on the patterned membrane surface was lower than that of non-patterned membrane. However, unlike previous 2 μm latex particles test, it is surprising that the antifouling effect of 25 μm prism pattern was significantly increased. Thus, if the feed consist of large size of foulant, the small size pattern could have high antifouling ability.

- The mass of deposited latex particle in interval prism pattern was even higher than that of non-patterned membrane. It is because the area of valley region of 1:2 interval prism patterns was 5 times higher than that of no-interval prism pattern. Therefore, under slow Reynolds conditions, introducing the interval between prism patterns was unnecessary.

- Increasing the Reynolds number from 600 to 1600, the deposition of latex particle in interval prism pattern was dramatically decreased. We could assume that the additional shear and vortex was generated in interval prism pattern. As a future work, it is necessary to analysis the additional shear stress and vortex formation using modeling tools.

VI. 초 록

높은 수질의 물을 제공하는 분리막을 이용한 수처리 공정에서는, 대부분 분리막 표면에 형성되는 막오염으로 인해 분리막의 성능이 지속적으로 저하되는 문제점을 가지고 있다. 최근 들어 이러한 막오염 문제를 해결하기 위해, 분리막의 표면에 다양한 모양의 패턴을 부가하여 입자의 침착을 방해하고 분리막의 투수 성능을 향상시키는 연구가 진행되고 있다. 하지만 기존의 연구에서는 적용할 수 있는 패턴의 모양이 한정적이며, 패턴의 구현도에는 큰 관심을 두지 않았다. 또한 패턴의 막오염 저감 효과에 관한 메커니즘은 아직 알려진 바가 없다. 이에 본 연구에서는, 새로운 패턴형 분리막 제조 기법을 개발하고, 패턴형 분리막의 막오염 저감 효과를 체계적으로 분석하고자 하였다.

첫 번째로는, 다양한 모양의 패턴을 적용할 수 있는 막 제조 공정을 개발하였다. 다양한 패턴의 몰드를 기판으로 사용하여 고분자 용액을 도포하고, 비용매에 침지하여 상전이를 유도 하였다. 이 결과 프리즘, 엠보싱, 피라미드 등의 다양한 표면 구조를 갖는 패턴형 분리막을 제조 할 수 있었다. 또한 분리막 제조 과정에서 제조에 영향을 주는 인자와 패턴의 구현도 사이의 상관관계를 규명하였다.

두 번째로는, 제조한 분리막의 막 특성을 평가하고, 기본적인 막 성능을 실험실 규모의 막공정을 통해 확인하였다. 그 결과 패턴형 분리막은 공극 크기 분포가 약 0.6 – 0.9 μm 로 정밀여과막에 해당하며, 이 공극 크기 분포는 패턴의 모양과는 관계가 없었다. 이외에도 패턴형 분리막의 단면 구조 또한 패턴의 모양에 관계없이 유사하였다. 패턴형 분리막은 표면의 패턴으로 인해 패턴이 없

는 분리막보다 약 20%의 투수도 향상을 보였으며, 막오염도 크게 저감하는 것을 실험실 규모의 교차흐름 반응기를 통해 확인하였다. 그러나 패턴형 분리막이 잘 만들어지지 못하여 패턴의 높이가 감소하면, 그 성능이 감소하는 것을 확인하였다.

마지막으로, 패턴형 분리막에서 패턴의 막오염 억제 메커니즘을 분석하였다. 패턴의 크기와 모양 및 오염물의 크기를 다르게 하여 다양한 조건에서 패턴형 분리막의 막저감 효과를 관찰하였다. 그 결과 오염물의 크기가 클 때는 패턴의 크기가 작은 것이 막오염 저감에 효과적이였으며, 대부분의 경우에서 유속이 빠를 때, 패턴의 막오염 저감 효과가 높게 나타났다. 또한 패턴과 패턴사이에 인터벌을 부가하면, 오염물이 쉽게 쌓일 수 있는 패턴의 골 부분의 모양이 변하기 때문에 추가적인 막오염 억제 효과가 나타나는 것을 확인하였다.

패턴형 분리막의 제막 및 실험실 규모에서의 성능평가는 이 기술이 차후 다양한 수처리 시스템 또는 환경공학 시스템에 적용될 수 있는 가능성을 보여주었다.

주요어: 분리막공정, 패턴형 분리막, 막오염 제어, 리소그래피

학 번: 2007-30850

Reference

Altena, F.W. and Smolders, C.A. (1982) Calculation of Liquid Liquid-Phase Separation in a Ternary-System of a Polymer in a Mixture of a Solvent and a Nonsolvent. Macromolecules 15(6), 1491-1497.

Altena, F.W., Schroder, J.S., Vandehuls, R. and Smolders, C.A. (1986) Thermoreversible Gelation of Cellulose-Acetate Solutions Studied by Differential Scanning Calorimetry. Journal of Polymer Science Part B-Polymer Physics 24(8), 1725-1734.

APHA (1998) Standard Methods for the Examination of Water and Wastewater, American Public Health Association, Washington, DC.

Bessonov, A., Seo, J.W., Kim, J.G., Hwang, E.S., Lee, J.W., Cho, J.W., Kim, D.J. and Lee, S. (2011) Control over pattern fidelity and surface wettability of imprinted templates for flexible color filter manufacturing. Microelectronic Engineering 88(9), 2913-2918.

Bikel, M., Punt, I.G.M., Lammertink, R.G.H. and Wessling, M. (2009) Micropatterned Polymer Films by Vapor-Induced Phase Separation Using Permeable Molds. Acs Applied Materials & Interfaces 1(12), 2856-2861.

Bottino, A., Cameraroda, G., Capannelli, G. and Munari, S. (1991) The Formation of Microporous Polyvinylidene Difluoride Membranes by Phase-Separation. Journal of Membrane Science 57(1), 1-20.

Brittain, S., Paul, K., Zhao, X.M. and Whitesides, G. (1998a) Soft lithography and microfabrication. Physics World 11(5), 31-36.

Brittain, S.T., Kenis, P.J.A., Schueller, O.J.A., Jackman, R.J. and Whitesides, G.M. (1998b) The use of soft lithography for the fabrication of components for micro electromechanical systems (MEMS). Abstracts of Papers of the American Chemical Society 216, U312-U312.

Broens, L., Koenhen, D.M. and Smolders, C.A. (1977) Mechanism of Formation of Asymmetric Ultrafiltration and Hyperfiltration Membranes. Desalination 22(1-3), 205-219.

Caneba, G.T. and Soong, D.S. (1985) Polymer Membrane Formation through the

Thermal-Inversion Process .2. Mathematical-Modeling of Membrane-Structure Formation. Macromolecules 18(12), 2545-2555.

Choi, S.J., Yoo, P.J., Baek, S.J., Kim, T.W. and Lee, H.H. (2004) An ultraviolet-curable mold for sub-100-nm lithography. Journal of the American Chemical Society 126(25), 7744-7745.

Choi, K.M. and Rogers, J.A. (2003) A photocurable poly(dimethylsiloxane) chemistry designed for soft lithographic molding and printing in the nanometer regime. Journal of the American Chemical Society 125(14), 4060-4061.

Choi, D.C., Won, Y.J., Lee, C.H., Lee, S., Lee, M.H. and Khang, D.Y. (2013) Tunable pore size micro/submicron-sieve membranes by soft lithography. Journal of Materials Chemistry A 1(40), 12448-12454.

Culfaz, P.Z., Buetehorn, S., Utiu, L., Kueppers, M., Bluemich, B., Melin, T., Wessling, M. and Lammertink, R.G.H. (2011a) Fouling Behavior of Microstructured Hollow Fiber Membranes in Dead-End Filtrations: Critical Flux Determination and NMR Imaging of Particle Deposition. Langmuir 27(5), 1643-1652.

Culfaz, P.Z., Haddad, M., Wessling, M. and Lammertink, R.G.H. (2011b) Fouling behavior of microstructured hollow fibers in cross-flow filtrations: Critical flux determination and direct visual observation of particle deposition. Journal of Membrane Science 372(1-2), 210-218.

Culfaz, P.Z., Rolevink, E., van Rijn, C., Lammertink, R.G.H. and Wessling, M. (2010) Microstructured hollow fibers for ultrafiltration. Journal of Membrane Science 347(1-2), 32-41.

Culfaz, P.Z., Wessling, M. and Lammertink, R.G.H. (2011c) Hollow fiber ultrafiltration membranes with microstructured inner skin. Journal of Membrane Science 369(1-2), 221-227.

Culfaz, P.Z., Wessling, M. and Lammertink, R.G.H. (2011d) Fouling behavior of microstructured hollow fiber membranes in submerged and aerated filtrations. Water Research 45(4), 1865-1871.

Dai, M.T., Lam, K.Y., Chen, H.J.H. and Huang, F.S. (2007) Nanocontact printing using a hydrogen silsesquioxane stamp with low E-beam dose. Journal of the Electrochemical Society 154(7), H636-H641.

Drews, A. (2010) Membrane fouling in membrane bioreactors-Characterisation,

contradictions, cause and cures. Journal of Membrane Science 363(1-2), 1-28.

Efimenko, K., Finlay, J., Callow, M.E., Callow, J.A. and Genzer, J. (2009) Development and Testing of Hierarchically Wrinkled Coatings for Marine Antifouling. Acs Applied Materials & Interfaces 1(5), 1031-1040.

Escobar, I.C. and Schäfer, A.I. (2010) Sustainable water for the future : water recycling versus desalination, Elsevier Science, Amsterdam ; Boston.

Enegess, D., Togna, A.P. and Sutton, P.M. (2003) Membrane separation applications to biosystems for wastewater treatment. Filtration & Separation 40(1), 14-17.

Frank, F.C. and Keller, A. (1988) 2-Fluid Phase-Separation - Modified by a Glass-Transition. Polymer Communications 29(7), 186-189.

Gittens, G.J., Hitchcoc.Pa, Sammon, D.C. and Wakley, G.E. (1970) Structure of Cellulose Acetate Membranes for Reverse Osmosis .1. Membranes Prepared from a Dioxan Based Dope. Desalination 8(3), 369-&.

Hanks, P.L. and Lloyd, D.R. (2007) Deterministic model for matrix solidification in liquid-liquid thermally induced phase separation. Journal of Membrane Science 306(1-2), 125-133.

Hiatt, W.C., Vitzthum, G.H. and Wagener, K.B. (1984) Microporous Membranes Via Upper Critical-Temperature Phase-Separation. Abstracts of Papers of the American Chemical Society 187(Apr), 35-Pmse.

Hiatt, W.C., Vitzthum, G.H., Wagener, K.B., Gerlach, K. and Josefiak, C. (1985) Microporous Membranes Via Upper Critical-Temperature Phase-Separation. ACS Symposium Series 269, 229-244.

Reuvers, A.J. and Smolders, C.A. (1987) Formation of Membranes by Means of Immersion Precipitation .2. The Mechanism of Formation of Membranes Prepared from the System Cellulose-Acetate Acetone Water. Journal of Membrane Science 34(1), 67-86.

Ho, J.M., Beck, R.G., Westervelt, R.M. and Whitesides, G.M. (1998) The use of soft lithography to fabricate arrays of Schottky diodes. Advanced Materials 10(8), 574-+.

Hong, P.S. and Lee, H.H. (2003) Pattern uniformity control in room-temperature imprint lithography. Applied Physics Letters 83(12), 2441-2443.

Hua, F., Gaur, A., Sun, Y.G., Word, M., Jin, N., Adesida, I., Shim, M., Shim, A. and Rogers, J.A. (2006) Processing dependent behavior of soft imprint lithography on the 1--10-nm scale. Ieee Transactions on Nanotechnology 5(3), 301-308.

Hua, F., Sun, Y.G., Gaur, A., Meitl, M.A., Bilhaut, L., Rotkina, L., Wang, J.F., Geil, P., Shim, M., Rogers, J.A. and Shim, A. (2004) Polymer imprint lithography with molecular-scale resolution. Nano Letters 4(12), 2467-2471.

Hui, C.Y., Jagota, A., Lin, Y.Y. and Kramer, E.J. (2002) Constraints on microcontact printing imposed by stamp deformation. Langmuir 18(4), 1394-1407.

Lee, J.N., Park, C. and Whitesides, G.M. (2003) Solvent compatibility of poly(dimethylsiloxane)-based microfluidic devices. Analytical Chemistry 75(23), 6544-6554.

Hwang, B.K., Lee, W.N., Yeon, K.M., Park, P.K., Lee, C.H., Chang, I.S., Drews, A. and Kraume, M. (2008) Correlating TMP increases with microbial characteristics in the bio-cake on the membrane surface in a membrane bioreactor. Environmental Science & Technology 42(11), 3963-3968.

Jeon, N.L., Hu, J.M., Whitesides, G.M., Erhardt, M.K. and Nuzzo, R.G. (1998) Fabrication of silicon MOSFETs using soft lithography. Advanced Materials 10(17), 1466-1469.

Judd, S. and Judd, C. (2011) The MBR book : principles and applications of membrane bioreactors in water and wastewater treatment, Elsevier, Amsterdam ; Boston.

Kamide, K. and Matsuda, S. (1984) Phase-Equilibria of Quasi-Ternary Systems Consisting of Multicomponent Polymers in a Binary Solvent Mixture .2. Role of Initial Concentration and Relative Amount of Polymers Partitioned in 2 Phases. Polymer Journal 16(7), 515-530.

Kesting, R.E. (1990) The 4 Tiers of Structure in Integrally Skinned Phase Inversion Membranes and Their Relevance to the Various Separation Regimes. Journal of Applied Polymer Science 41(11-12), 2739-2752.

Khang, D.Y. and Lee, H.H. (2000) Room-temperature imprint lithography by solvent vapor treatment. Applied Physics Letters 76(7), 870-872.

Khang, D.Y., Yoon, H. and Lee, H.H. (2001) Room-temperature imprint lithography. Advanced Materials 13(10), 749-752.

Khang, D.Y., Kang, H., Kim, T. and Lee, H.H. (2004) Low-pressure nanoimprint lithography. Nano Letters 4(4), 633-637.

Khang, D.Y. and Lee, H.H. (2004a) Sub-100 nm patterning with an amorphous fluoropolymer mold. Langmuir 20(6), 2445-2448.

Khang, D.Y. and Lee, H.H. (2004b) Pressure-assisted capillary force lithography. Advanced Materials 16(2), 176-+.

Koningsv.R (1972) Liquid Liquid Equilibria in Quasi-Ternary Systems. Chemicke Zvesti 26(3), 263-&.

Koenhen, D.M., Mulder, M.H.V. and Smolders, C.A. (1977) Phase Separation Phenomena during Formation of Asymmetric Membranes. Journal of Applied Polymer Science 21(1), 199-215.

Kimmerle, K. and Strathmann, H. (1990) Analysis of the Structure-Determining Process of Phase Inversion Membranes. Desalination 79(2-3), 283-302.

Kim, E., Xia, Y.N. and Whitesides, G.M. (1996) Micromolding in capillaries: Applications in materials science. Journal of the American Chemical Society 118(24), 5722-5731.

Kim, Y.S., Suh, K.Y. and Lee, H.H. (2001) Fabrication of three-dimensional microstructures by soft molding. Applied Physics Letters 79(14), 2285-2287.

Kim, J.H., Choi, D.C., Yeon, K.M., Kim, S.R. and Lee, C.H. (2011) Enzyme-Immobilized Nanofiltration Membrane To Mitigate Biofouling Based on Quorum Quenching. Environmental Science & Technology 45(4), 1601-1607.

Kumar, A., Biebuyck, H.A. and Whitesides, G.M. (1994) Patterning Self-Assembled Monolayers - Applications in Materials Science. Langmuir 10(5), 1498-1511.

Kumar, A. and Whitesides, G.M. (1993) Features of Gold Having Micrometer to Centimeter Dimensions Can Be Formed through a Combination of Stamping with an Elastomeric Stamp and an Alkanethiol Ink Followed by Chemical Etching. Applied Physics Letters 63(14), 2002-2004.

Lai, K.L., Leu, I.C. and Hon, M.H. (2009) Soft imprint lithography using swelling/deswelling characteristics of a polymer mold and a resist induced by a poor solvent. Journal of Micromechanics and Microengineering 19(3).

Lang, W.Z., Shen, J.P., Wei, Y.T., Wu, Q.Y., Wang, J. and Guo, Y.J. (2013) Precipitation kinetics, morphologies, and properties of poly(vinyl butyral) hollow fiber ultrafiltration membranes with respect to polyvinylpyrrolidone molecular weight. Chemical Engineering Journal 225, 25-33.

Li, D.M., Krantz, W.B., Greenberg, A.R. and Sani, R.L. (2006) Membrane formation via thermally induced phase separation (TIPS): Model development and validation. Journal of Membrane Science 279(1-2), 50-60.

Li, X.F., Wang, Y.G., Lu, X.L. and Xiao, C.F. (2008) Morphology changes of polyvinylidene fluoride membrane under different phase separation mechanisms. Journal of Membrane Science 320(1-2), 477-482.

Li, H.W., Muir, B.V.O., Fichet, G. and Huck, W.T.S. (2003) Nanocontact printing: A route to sub-50-nm-scale chemical and biological patterning. Langmuir 19(6), 1963-1965.

Lim, H., Choi, K.B., Kim, G., Park, S., Ryu, J. and Lee, J. (2011) Roller nanoimprint lithography for flexible electronic devices of a sub-micron scale. Microelectronic Engineering 88(8), 2017-2020.

Lim, H., Kim, G., Choi, K.B., Jeong, M., Ryu, J. and Lee, J. (2012) Nanoimprint lithography with a soft roller and focused UV light for flexible substrates. Microelectronic Engineering 98, 279-283.

Manabe, S., Kamata, Y., Iijima, H. and Kamide, K. (1987) Some Morphological-Characteristics of Porous Polymeric Membranes Prepared by Microphase Separation Method. Polymer Journal 19(4), 391-404.

Mulder, M.H.V., Hendrikman, J.O., Wijmans, J.G. and Smolders, C.A. (1985) A Rationale for the Preparation of Asymmetric Pervaporation Membranes. Journal of Applied Polymer Science 30(7), 2805-2820.

M.T., Eirich, F.R., Strathma.H and Baker, R.W. (1973) Preparation of Asymmetric Loeb-Sourirajan Membranes. Journal of Polymer Science Part C-Polymer Letters 11(3), 201-205.

Odom, T.W., Love, J.C., Wolfe, D.B., Paul, K.E. and Whitesides, G.M. (2002) Improved pattern transfer in soft lithography using composite stamps. Langmuir 18(13), 5314-5320.

Park, Y.J., Kang, Y.S. and Park, C.M. (2005) Micropatterning of semicrystalline poly(vinylidene fluoride) (PVDF) solutions. European Polymer Journal 41(5),

1002-1012.

Park, H.H., Lim, H., Lee, S. and Lee, J. (2012) Fabrication of an adhesion-free transparent roll stamp for large area patterning using ultraviolet-type roller nanoimprint lithography. Journal of Vacuum Science & Technology B 30(6).

Peters, A.M., Lammertink, R.G.H. and Wessling, M. (2008) Comparing flat and micro-patterned surfaces: Gas permeation and tensile stress measurements. Journal of Membrane Science 320(1-2), 173-178.

Radovanovic, P., Thiel, S.W. and Hwang, S.T. (1992a) Formation of Asymmetric Polysulfone Membranes by Immersion Precipitation .1. Modeling Mass-Transport during Gelation. Journal of Membrane Science 65(3), 213-229.

Radovanovic, P., Thiel, S.W. and Hwang, S.T. (1992b) Formation of Asymmetric Polysulfone Membranes by Immersion Precipitation .2. The Effects of Casting Solution and Gelation Bath Compositions on Membrane-Structure and Skin Formation. Journal of Membrane Science 65(3), 231-246.

Rogers, J.A. and Lee, H.H. (2009) Unconventional nanopatterning techniques and applications, Wiley, Hoboken, N.J.

Ruchhoeft, P., Colburn, M., Choi, B., Nounu, H., Johnson, S., Bailey, T., Damle, S., Stewart, M., Ekerdt, J., Sreenivasan, S.V., Wolfe, J.C. and Willson, C.G. (1999) Patterning curved surfaces: Template generation by ion beam proximity lithography and relief transfer by step and flash imprint lithography. Journal of Vacuum Science & Technology B 17(6), 2965-2969.

Reuvers, A.J., Vandenberg, J.W.A. and Smolders, C.A. (1987) Formation of Membranes by Means of Immersion Precipitation .1. A Model to Describe Mass-Transfer during Immersion Precipitation. Journal of Membrane Science 34(1), 45-65.

Reuvers, A.J., Altena, F.W. and Smolders, C.A. (1986) Demixing and Gelation Behavior of Ternary Cellulose-Acetate Solutions. Journal of Polymer Science Part B-Polymer Physics 24(4), 793-804.

Rolland, J.P., Hagberg, E.C., Denison, G.M., Carter, K.R. and DeSimone, J.M. (2004a) High-resolution soft lithography: Enabling materials for nanotechnologies. Angewandte Chemie-International Edition 43(43), 5796-5799.

Rolland, J.P., Van Dam, R.M., Schorzman, D.A., Sr, Q. and DeSimone, J.M.

(2004b) Solvent resistant photocurable "liquid teflon" for microfluidic device fabrication (vol 126, pg 2322, 2004). Journal of the American Chemical Society 126(26), 8349-8349.

Strathmann, H. (1985) Production of Microporous Media by Phase Inversion Processes. ACS Symposium Series 269, 165-195.

Schmid, H. and Michel, B. (2000) Siloxane polymers for high-resolution, high-accuracy soft lithography. Macromolecules 33(8), 3042-3049.

Sharp, K.G., Blackman, G.S., Glassmaker, N.J., Jagota, A. and Hui, C.Y. (2004) Effect of stamp deformation on the quality of microcontact printing: Theory and experiment. Langmuir 20(15), 6430-6438.

Song, S., Khang, D.Y., Kim, M.J., Park, J.E. and Lee, H.H. (2007) Asymmetric porous thin film preparation by controlled solvent absorption using PDMS. Journal of Membrane Science 305(1-2), 5-12.

Strathmann, H. and Kock, K. (1977) Formation Mechanism of Phase Inversion Membranes. Desalination 21(3), 241-255.

Suh, K.Y., Kim, Y.S. and Lee, H.H. (2001) Capillary force lithography. Advanced Materials 13(18), 1386-1389.

Suh, K.Y. and Lee, H.H. (2002) Capillary force lithography: Large-area patterning, self-organization, and anisotropic dewetting. Advanced Functional Materials 12(6-7), 405-413.

Suh, K.Y., Langer, R. and Lahann, J. (2003) Fabrication of elastomeric stamps with polymer-reinforced sidewalls via chemically selective vapor deposition polymerization of poly(p-xylylene). Applied Physics Letters 83(20), 4250-4252.

Sze Chai Kwok, H.L.a.P.O.C. (2010) Water Technology Markets 2010: Key opportunities and emerging trends.

Termonia, Y. (1995) Fundamentals of Polymer Coagulation. Journal of Polymer Science Part B-Polymer Physics 33(2), 279-288.

Truong, T.T., Lin, R.S., Jeon, S., Lee, H.H., Maria, J., Gaur, A., Hua, F., Meinel, I. and Rogers, J.A. (2007) Soft lithography using acryloxy perfluoropolyether composite stamps. Langmuir 23(5), 2898-2905.

Takulapalli, B.R., Morrison, M.E., Gu, J. and Zhang, P.M. (2011) A nanocontact

printing system for sub-100 nm aligned patterning. Nanotechnology 22(28).

Tan, H., Gilbertson, A. and Chou, S.Y. (1998) Roller nanoimprint lithography. Journal of Vacuum Science & Technology B 16(6), 3926-3928.

Tsai, F.J. and Torkelson, J.M. (1990) Microporous Poly(Methyl Methacrylate) Membranes - Effect of a Low-Viscosity Solvent on the Formation Mechanism. Macromolecules 23(23), 4983-4989.

VandeWitte, P., Dijkstra, P.J., vandenBerg, J.W.A. and Feijen, J. (1996a) Phase separation processes in polymer solutions in relation to membrane formation. Journal of Membrane Science 117(1-2), 1-31.

VandeWitte, P., VandenBerg, J.W.A., Feijen, J., Reeve, J.L. and McHugh, A.J. (1996b) In situ analysis of solvent/nonsolvent exchange and phase separation processes during the membrane formation of polylactides. Journal of Applied Polymer Science 61(4), 685-695.

Vitagliano, V., Sartorio, R., Scala, S. and Spaduzzi, D. (1978) Diffusion in a Ternary-System and Critical Mixing Point. Journal of Solution Chemistry 7(8), 605-621.

Vogelaar, L., Barsema, J.N., van Rijn, C.J.M., Nijdam, W. and Wessling, M. (2003) Phase separation micromolding - PS mu M. Advanced Materials 15(16), 1385-+.

Wang, X.Y., Zhang, L., Sun, D.H., An, Q.F. and Chen, H.L. (2009) Formation mechanism and crystallization of poly(vinylidene fluoride) membrane via immersion precipitation method. Desalination 236(1-3), 170-178.

Won, Y.J., Lee, J., Choi, D.C., Chae, H.R., Kim, I., Lee, C.H. and Kim, I.C. (2012) Preparation and Application of Patterned Membranes for Wastewater Treatment. Environmental Science & Technology 46(20), 11021-11027.

Xia, Y.N. and Whitesides, G.M. (1995) Use of Controlled Reactive Spreading of Liquid Alkanethiol on the Surface of Gold to Modify the Size of Features Produced by Microcontact Printing. Journal of the American Chemical Society 117(11), 3274-3275.

Xia, Y.N., Tien, J., Qin, D. and Whitesides, G.M. (1996) Non-photolithographic methods for fabrication of elastomeric stamps for use in microcontact printing. Langmuir 12(16), 4033-4038.

Xia, Y.N. and Whitesides, G.M. (1998) Soft lithography. Angewandte Chemie-International Edition 37(5), 551-575.

Xiong, Y.H. and Liu, Y. (2010) Biological control of microbial attachment: a promising alternative for mitigating membrane biofouling. Applied Microbiology and Biotechnology 86(3), 825-837.

Yamamoto, K., Hiasa, M., Mahmood, T. and Matsuo, T. (1989) Direct Solid-Liquid Separation Using Hollow Fiber Membrane in an Activated-Sludge Aeration Tank. Water Science and Technology 21(4-5), 43-54.

Ye, X.D., Ding, Y.C., Duan, Y.G., Liu, H.Z. and Lu, B.H. (2010) Room-temperature capillary-imprint lithography for making micro-/nanostructures in large areas. Journal of Vacuum Science & Technology B 28(1), 138-142.

Yeon, K.M., Lee, C.H. and Kim, J. (2009) Magnetic enzyme carrier for effective biofouling control in the membrane bioreactor based on enzymatic quorum quenching. Environmental Science & Technology 43(19), 7403-7409.

Yilmaz, L. and Mchugh, A.J. (1986) Analysis of Nonsolvent Solvent Polymer Phase-Diagrams and Their Relevance to Membrane Formation Modeling. Journal of Applied Polymer Science 31(4), 997-1018.

Yoon, H., Lee, K.M., Khang, D.Y., Lee, H.H. and Choi, S.J. (2004) Rapid flash patterning of nanostructures. Applied Physics Letters 85(10), 1793-1795.

Yoon, H., Kim, T.I., Choi, S.J., Suh, K.Y., Kim, M.J. and Lee, H.H. (2006) Capillary force lithography with impermeable molds. Applied Physics Letters 88(25).

Yoo, P.J., Choi, S.J., Kim, J.H., Suh, D., Baek, S.J., Kim, T.W. and Lee, H.H. (2004) Unconventional patterning with a modulus-tunable mold: From imprinting to microcontact printing. Chemistry of Materials 16(24), 5000-5005.

Zhenxin, Z. and Matsuura, T. (1991) Discussions on the Formation Mechanism of Surface Pores in Reverse-Osmosis, Ultrafiltration, and Microfiltration Membranes Prepared by Phase Inversion Process. Journal of Colloid and Interface Science 147(2), 307-315.